ADVANCED MATERIALS

Supporting Information

for *Adv. Mater.*, DOI 10.1002/adma.202308392

Robust Molecular Anodes for Electrocatalytic Water Oxidation Based on Electropolymerized Molecular Cu Complexes

Sebastian Amthor, Koushik Ranu, Carlos G. Bellido, Fernando F. Salomón, Alberto Piccioni, Raffaello Mazzaro, Federico Boscherini, Luca Pasquini, Marcos Gil-Sepulcre and Antoni Llobet**

Supporting information for

Robust Molecular Anodes for Electrocatalytic Water Oxidation Based on Electropolymerized Molecular Cu Complexes

Sebastian Amthor[1,+], Koushik Ranu[1,+], Carlos G. Bellido[1], Fernando F. Salomón[1], Alberto Piccioni[2], Raffaello Mazzaro[2], Federico Boscherini[2], Luca Pasquini[2], Marcos Gil-Sepulcre[1]*, Antoni Llobet[1,3]*.

[1] Institute of Chemical Research of Catalonia (ICIQ), Barcelona Institute of Science and Technology (BIST), Tarragona, Spain, Avinguda Països Catalans 16, 43007 Tarragona, Spain.

[2] Department of Physics and Astronomy, Alma Mater Studiorum – Università di Bologna, viale C. Berti Pichat 6/2, 40127 Bologna, Italy

[3] Departament de Química, Universitat Autònoma de Barcelona, 08193 Cerdanyola del Vallès, Barcelona, Spain.

*Corresponding authors:

Antoni Llobet, Email: allobet@iciq.cat

Marcos Gil-Sepulcre, Email: mgil@iciq.es

Table of Contents

Materials

All chemicals used in this work were obtained from Sigma Aldrich and have been used without further purification unless explicitly indicated. Multi-walled carbon nanotubes (**CNT**) were purchased from HeJi, Inc. (China) with >95% purity, length ~10 µm and OD > 50 nm. Glassy carbon (**GC**) electrodes were purchased from CHI instruments. GC plate electrodes (**GC_p**, 20 x 10 x 0.18 mm) SIGRADUR® were purchased from HTW, Germany. Carbon paper electrodes (**CP**, SGL Carbon, Sigracet 39 AA) and Graphite felt (**GF**) electrodes were purchased from Fuel Cell Store. The solvents were selected to be HPLC grade and high-purity water was acquired by passing distilled water through a Nanopure MilliQ water purification system. All the synthetic procedures were performed under argon atmosphere using vacuum-line techniques, if not stated otherwise. For other spectroscopic and electrochemical studies HPLC grade solvents were used.

Instrumentation

pH meter: The pH of all solutions was measured using a Mettler Toledo Seven Compact pH meter calibrated before measurements through standard solutions at pH 4.0, 7.0 and 9.2.

NMR spectroscopy: ^{1}H (400 MHz) and ^{13}C (101 MHz) NMR spectra were recorded with a Bruker Avance 400 MHz spectrometer. All the measurements were carried out at room temperature in the corresponding deuterated solvent using residual protons as internal reference. NMR spectroscopic data were analyzed using MestreNova software.

Electrospray ionization mass spectra (ESI-MS) were performed on an Agilent Technologies 6130-Quadrupole LC/MS connected to an Agilent Technologies HPLC-1200 series. Samples were dissolved in the appropriate solvent and injected directly with an auto-sampler.

Elemental Analysis of the samples was carried out in a Thermo Finnigan elemental analyzer Flash 1112 model.

UV-vis spectrometry: A Cary 50 (Varian) UV-vis spectrophotometer was used to carry out the UV-vis spectroscopy. All the measurements were performed using a standard 1 cm pathway UV-vis cuvette.

Electrochemical measurements

All electrochemical experiments were conducted using a Cambria CHI 730 or CHI 660 bi-potentiostat, using a one-compartment three-electrode cell for cyclic voltammetry (CV) and differential pulse voltammetry (DPV) techniques and two compartment three-electrode set up for controlled potential electrolysis (CPE) experiments. A glassy carbon (GC, ϕ = 0.3 cm, S = 0.078 cm^2), carbon paper (CP, S = 0.5 cm^2) or graphite felt (GF, S = 1 cm^2) were employed as working electrodes (WE), a platinum disk (ϕ = 0.2 cm, S = 0.03 cm^2) or mesh as counter electrode (CE), and a Hg/Hg_2SO_4 (sat. K_2SO_4) as reference electrode (RE). The working electrodes were first polished with 0.05 µm alumina paste and rinsed with water and acetone. The CVs were iR compensated (85 %, as recommended in *ACS Energy Lett*. 2023, 8, 1952−1958) unless stated otherwise using the

automatic iR compensation protocol implemented in the CHI potentiostat. For low current densities, we routinely use 85 % compensation as recommended in CVs were recorded at 50 $mV \cdot s^{-1}$ unless otherwise stated. All the potentials reported in this work were converted to NHE by adding 0.65 V to the measured potential or versus ferrocene for organic solvents by addition of Ferrocene as internal standard at the end of the experiment.

Cyclic voltammetry and controlled potential electrolysis experiments

For cyclic voltammetry 20 mL vials were used as electrochemical cell. They were closed with a Teflon cap with inlets for the electrodes and for gas inlet and outlet. The scan rate was typically 50 $mV \cdot s^{-1}$ unless otherwise stated. DPV experiments were performed by using the following parameters, ΔE = 4 mV, amplitude = 50 mV, pulse width = 0.05 s, sampling width = 0.0167 s, pulse period = 0.2 s. CPE experiments were carried out in a 10 mL two compartment H-Cell separated with a frit applying the corresponding potential. One compartment was equipped with WE and RE electrodes together with a magnetic stirring bar. The counter compartment contained the CE electrode and a stirring bar.

Rotating-ring disk electrode (RRDE) experiments

RRDE experiments were conducted using a RRDE-3A from IJ-Cambria with an electrode composed of a GC disk (WE1) and a Pt ring (WE2) electrode (ϕ_{Disk} = 4 mm, S = 0.126 cm^2 and Pt ring: $\phi_{outer\text{-}Ring}$ = 7 mm, $\phi_{inner\text{-}Ring}$ = 5 mm, Figure S24) in a phosphate buffer 0.1 M pH 7 solution. A Pt disk electrode was used as CE and a Hg/Hg_2SO_4 (K_2SO_4 saturated) as RE. The electrochemical set-up consisted of a one-compartment cell equipped with a Teflon cap. The solution was purged with nitrogen for 20 min before each experiment to remove the O_2. The electrodes were connected to an IJ-Cambria CHI-730 bipotentiostat for electrochemical measurements. The rotation was set to 1600 rpm. An LSV experiment at a scan rate of 10 mVs^{-1} was conducted while the Pt ring electrode was set to a fixed potential of E_{app} = -0.5 V *vs.* NHE (estimated from previous CV experiments).

Preparation of the buffers

Phosphate buffer solution at pH 7.1 (I = 0.1 M) was prepared by dissolving NaH_2PO_4 (0.462 g, 3.8 mmol) and Na_2HPO_4 (0.754 g, 5.2 mmol) in 1 L of Mili-Q water.

Determination of Faradaic efficiency

Faradaic efficiency was obtained by comparing the ring currents (ratio of Pt ring current and GC disk current, compare Equation S1) of the modified electrodes to glassy carbon electrodes with drop casted RuO_2 particles, which were assumed to have 100% FE, during RRDE experiments. The potential of the Pt ring was set to the potential at which the oxygen reduction occurred (-0.5 V *vs.* NHE, Figure S24). A baseline correction based on the increased current of **GC/CNT@p-[LCu]$^{2-}$** was done at a potential of 0.75 V *vs.* NHE, which corrected the current by subtraction of 0.3 mA cm^{-2} at the peak current at 1.3 V *vs.* NHE for **GC/CNT@p-[LCu]$^{2-}$** (see Figure 4 of main manuscript). The values retrieved by eq. S1 are shown in eq. S2.

$$\frac{\frac{i_r Cu}{i_d Cu}}{\frac{i_r RuO_2}{i_d RuO_2}} \cdot 100 = \varepsilon \qquad \text{(S1)}$$

$$\frac{0.116}{0.115} \cdot 100 = 100\% \qquad \text{(S2)}$$

Where i_rCu and i_dCu are defined as Cu(III/II) cathodic and anodic currents (respectively) from **GC/CNT@p-[LCu]$^{2-}$** RRDE studies, while i_rRuO$_2$ and i_dRuO$_2$ are Ru(III/II) analogous currents from RRDE studies of RuO$_2$-dropcasted glassy carbon electrodes.

Surface loading

Surface loadings were determined by integration of the anodic and cathodic peak of the Cu(III/II) wave in the CVs (*i* vs t) after electropolymerization from the charge obtained, Q_{av}. The coverage Γ was calculated following the equation:

$$\Gamma\ (mol \cdot cm^{-2}) = \frac{Q_{av}}{F\ n_e\ A} \qquad \text{(S3a)}$$

$$Q_{av} = \frac{Q_{ap\ CuIII/II} + Q_{cp\ CuIII/II}}{2} \qquad \text{(S3b)}$$

Q_{av} is the charge under a peak of the reversible, one-electron wave obtained by integration of the cyclic voltammogram (average values of Cu(III/II) wave, see Equation S4); n_e is the number of electrons involved in that process, which is 1 for **[LCu]$^{2-}$**; *A* is the electrode and *F* is the Faradaic constant (96485 C·mol^{-1}).

Foot-Of-the-Wave-Analysis (FOWA)[1a]

Under catalytic conditions:

$$\frac{i}{Q_{Cu}} = \frac{k_{WNA}}{1+\exp(\frac{F(E-E^O)}{RT})} \qquad \text{(S4)}$$

Where *i* is the CV current intensity in the presence of the substrate; Q_{Cu} is the average of the charge for anodic and cathodic waves of the non-catalytic Cu(III/II) redox couple; *F* is the Faradaic constant; *E* is the scanning potential; *R* is 8.314 J mol^{-1} K^{-1}; *T* is 298 K and E^o is the apparent potential for the catalysis redox couple, extracted from DPV of the

same electrode. The value of k_{WNA} is equivalent to TOF_{MAX} (s^{-1}) in the used electrocatalytic scheme. TOF_{MAX} is the maximum turnover frequency (s^{-1}) that a molecule can catalyze the water oxidation reaction when *E* tends to infinite potential.[1b]

Atomic force microscopy (AFM)

AFM measurements were performed under ambient conditions using a Agilent 5500 system operating in tapping mode in air. Silicon cantilevers (OMCL-AC240TS, Olympus) were used. The AFM sample was prepared by electropolymerizing **$[LCu]^{2-}$** on a flat and polished GC plate electrodes (GC_p, 20 x 10 x 0.18 mm) SIGRADUR®.

Scanning electron microscopy (SEM) and energy-dispersive X-ray spectroscopy (EDX)

SEM images were recorded using a Quanta 600 from FEI company. For the energy dispersive X-ray analysis (EDX) the same SEM instrument was used. The SEM sample was prepared by electropolymerizing **$[LCu]^{2-}$** on CNT previously dropcasted on GC plate electrodes (GC_p, 20 x 10 x 0.18 mm) SIGRADUR®.

X-ray absorption spectroscopy (XAS)

Cu K-edge X-ray Absorption Spectroscopy measurements were performed on the LISA BM-08 beamline at ESRF, Grenoble, using fluorescence mode.[2]

Analysis of EXAFS signal was performed by using ATHENA.[3] The structural model used to fit the EXAFS data was taken from a related system reported in the literature[4] as cif file of **$[(Mac)Cu]^{2-}$** system (structure number 1959710). The calculation of the possible scattering paths that give a significant contribution to the EXAFS signal was performed using the FEFF[5] code built in ARTEMIS[37] software. Both single scattering (SS) and multiple scattering (MS) paths were considered in order to have a reliable representation of the EXAFS spectrum.[6] In this regard, only intra-molecular paths were considered, neglecting contributions coming from other molecules. In Table S1 we report the paths used for fitting the data and Figure S26 reports their pictorial representation. The fit was calculated adopting the following procedure: we started from the first shell, represented by the single scattering path 1, with an effective distance of 1.904 Å. In the Fourier transform, this shell is represented by the peak centered at ≈1.4 Å. The r-window used for this fit was 1-2 Å. Then we moved to the second shell. In this case, the second shell is represented by the broad peak at ≈2.1 Å, which is given by the contribution of two single scattering paths, namely 2 and 3, with an effective distance of 2.762 and 2.844 Å, respectively. The r-window used for this fit was 1-3.2 Å. Finally, we performed the final fit including also the third shell, represented by the single scattering path 4, with an effective distance of 3.983 Å. The r-window used for this fit was 1-3.9 Å. In addition, due to the planar geometry of the molecule, multi scattering paths were also considered. We found that among all the possible multi scattering paths calculated by FEFF simulation, path 5, with an effective distance of 3.035 Å, has to be included in the final fit to better reproduce the feature of the Fourier transform between 2 and 3 Å. To confirm the right choice of the paths, we report in Fig. S29 the contribution of each path to the final fit for

the sample $[LCu]^{2-}$ (other spectra are quite similar to this one). The fit was performed considering the Fourier transform of the EXAFS signal between 2–10 $Å^{-1}$, adopting a Hanning window and using 10 parameters for the refining procedure: a common shift of the energy origin (ΔE), independent variations of the path lengths (ΔR) and Debye Waller factors (σ^2), except for σ^2 for paths 2 and 3 which were constrained to be equal since they involve the same elements and in order to avoid too many fitting parameters. Since the aim of this analysis is to highlight differences in the local structure after different CPE times we fix the amplitude reduction factor S_0^2 to 1 for all fits in order to reduce the errors on the Debye Waller factors and the number of free parameters. This choice is justified by the difficulty, especially in when low Z atoms are present, in the determination of the amplitude reduction factor and the Debye Waller factors independently, since they are highly correlated in the fitting procedure. Models with different realistic values of the path degeneracies were tested, starting from those derived from the aforementioned cif file; we report in Table S1 the degeneracy values that give the best fit in terms of lowest R-factor. In Figure 2 of the main text, we display the best fit curves in in real space while the numerical values of the parameters are reported in Table S2.

Synthetic procedures

Synthesis of H_4L ligand

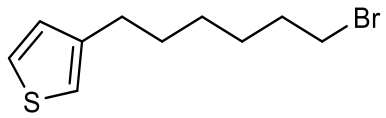

3-(6-bromohexyl)thiophene (**1**): To dry hexane (50 mL) *n*BuLi (6.25 mL, 1.6 M in hexane) was added under Argon and stirred for 10 min. Afterwards, THF (5 mL) and 3-bromothiophene (10.65 mmol, 1 mL) were added to the mixture and stirred for 1 h. Subsequently, 1,6-dibromohexane (106.5 mmol, 16 mL) was added and the solution was allowed to stir for 12 h at room temperature. After that time the solvent and the excess 1,6-dibromohexane were removed in vacuum at 65 °C (1 mbar). The crude yellow oil was purified using column chromatography (silica gel, hexane) to obtain **1** as a colorless oil. (886.5 mg, 33.7%). ^{1}H NMR (300 MHz, DMSO-d_6) δ 7.43 (dd, *J* = 4.9, 2.9 Hz, 1H), 7.17 – 7.09 (m, 1H), 6.98 (dd, *J* = 4.9, 1.3 Hz, 1H), 3.52 (t, *J* = 6.7 Hz, 2H), 2.58 (t, *J* = 7.6 Hz, 2H), 1.90 – 1.71 (m, 2H), 1.65-1.51 (m, 2H), 1.49 – 1.25 (m, 4H).

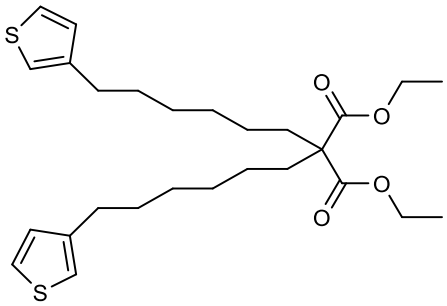

Diethyl 2,2-bis(6-(thiophen-3-yl)hexyl)malonate (**2**): To a stirring suspension of sodium hydride (95mg, 2.5mmol) in THF (10 mL) , diethylmalonate (190 mg, 0.18 mL, 1.18 mmol) was added slowly under inert atmosphere. Resulting mixture was stirred for 45min until it turned clear. Afterwards, **1** (580 mg, 2.35 mmol) was added to it and mixture was refluxed under inert atmosphere for 48 hours at 75 ºC. The formed NaBr was filtered off and the crude product was purified using column chromatography (silica gel, dichloromethane) to yield a colorless oil (700 mg, 60 %). ^{1}H NMR (300 MHz, $CDCl_3$) δ 7.25 (dd, *J* = 4.9, 3.0 Hz, 2H), 6.99 – 6.87 (m, 4H), 4.26 – 4.11 (m, 4H), 2.69 – 2.55 (m, 4H), 1.95 – 1.81 (m, 4H), 1.67 – 1.55 (m, 4H), 1.39 – 1.31 (m, 6H), 1.25 (t, *J* = 7.0 Hz, 8H), 1.21 – 1.09 (m, 4H). ^{1}H NMR (300 MHz, DMSO-d_6) δ 7.50 – 7.34 (m, 2H), 7.19 – 7.06 (m, 2H), 7.06 – 6.91 (m, 2H), 4.18 – 4.03 (m, 4H), 2.62 – 2.52 (m, 4H), 1.87 – 1.68 (m, 4H), 1.64 – 1.46 (m, 4H), 1.32 – 1.19(m, 12H), 1.23 – 1.11 (m, 6H).

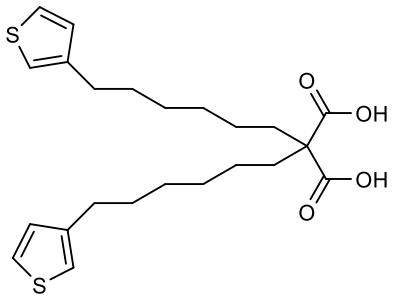

2,2-bis(6-(thiophen-3-yl)hexyl)malonic acid (**3**): To a stirring mixture of diethyl 2,2-bis(6-(thiophen-3-yl)hexyl)malonate (0.518 g, 1.18 mmol, **2**) in water (5 mL) and ethanol (5 mL) were added KOH pellets (0.80 g, 14 mmol). The solvent was removed in vacuum to a white powder. The solid was dissolved in water and extracted with diethyl ether. The aqueous layer was then acidified with concentrated HCl (12 mL) and extracted with diethyl ether (3 x 25 mL). The combined organic layers were dried over Na_2SO_4 and the solvent was removed under reduced pressure to yield **3** as a highly viscous off-white oil, which crystalizes over time. (340 mg, 65%). ^{1}H NMR (300 MHz, DMSO-d^6) δ7.50 – 7.37 (m, 2H), 7.12 (t, *J* = 3.9 Hz, 2H), 7.04 – 6.91 (m, 2H), 2.67 – 2.50 (m, 4H), 1.81 – 1.63 (m, 4H), 1.64 – 1.45 (m, 4H), 1.28 (s, 8H), 1.19 – 1.00 (m, 4H). ATR-IR [cm^{-1}]: 1701 (HO-C=O) (Figure S18).

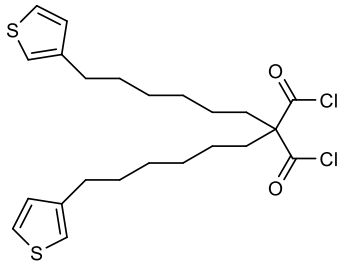

2,2-bis(6-(thiophen-3-yl)hexyl)malonyl dichloride (**4**): To a solution of 2,2-bis(6-(thiophen-3-yl)hexyl)malonic acid (500 mg, 1.15 mmol, **3**) in dry dichloromethane (30 mL) oxalyl chloride was added (0.24 mL, 2.4 eq). The mixture was stirred for 10 minutes after which time N,N-dimethylformamide was added (21 µL, 0.1 eq.). The mixture was allowed to stir at room temperature for 12 h under an Argon atmosphere. After that time the solvent and excess oxalyl chloride were removed in vacuum and the crude product was used immediately without further purification. ATR-IR [cm^{-1}]: 1801 (Cl-C=O) (Figure S18).

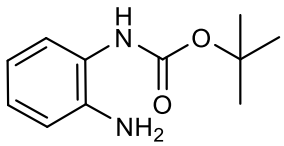

Tert-butyl(2-aminophenyl)carbamate (**5**): A mixture of *o*-phenylenediamine (270 mg, 2.5 mmol), $LiClO_4$ (80mg, 0.2 eq.) and Boc-anhydride (550 g, 2.5 mmol) was weighted in an oven dry round bottom flask and dissolved in dry dichloromethane (10 mL) under inert atmosphere. The solution was stirred for 12 h at room temperature. Afterwards, the suspension was filtered through a glass frit and the filtrate obtained was evaporated to dryness. The resulting residue was purified by column chromatography (silica as solid

support, EtOAc/Hexane 1:10). (495 mg, Yield: 99%) ^{1}H NMR (300 MHz, DMSO-d_6): δ 8.26 (s, 1H), 7.17 (d, J = 7.8 Hz, 1H), 6.83 (dd, J = 14.3, 7.9Hz, 7.3Hz, 1H), 6.67 (dd, J=8.0, 1.5 Hz,1H), 6.52(dd, J= 7.8, 1.5 Hz, 1H) 4.84 (s, 2H), 1.45 (s, 9H).

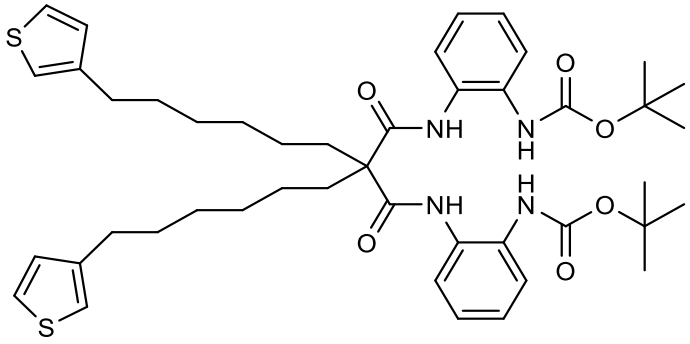

Di-tert-butyl(((2,2-bis(6-(thiophen-3-yl)hexyl)malonyl)bis(azanediyl))bis(2,1-phenylene)) dicarbamate (**6**): To a solution of tert-butyl (2-aminophenyl)carbamate (428 mg, 2.1 mmol) in dry THF (50 mL) and pyridine (215 µL, 2.7 mmol), 2,2-bis(6-(thiophen-3-yl)hexyl)malonyl dichloride (**4**) was slowly added dissolved in THF (50 mL) and the resulting mixture was stirred under inert atmosphere at room temperature for 12h. Afterwards, the solvent was removed under reduced pressure and the crude product was purified using column chromatography (silica gel, cyclohexane/EtOAc 5: 1) to yield a yellowish oil. (170mg, Yield: 20%). ^{1}H NMR (300 MHz, DMSO-d^6) δ 9.71 (s, 2H), 8.56 (s, 2H), 7.52 (d, *J* = 7.5 Hz, 2H), 7.45 (s, 2H), 7.40 (dd, *J* = 5.0, 3.1 Hz, 2H), 7.21 – 7.09 (m, 4H), 7.07 (s, 2H), 6.93 (d, *J* = 5.1 Hz, 2H), 2.06 – 1.91 (m, 4H), 1.61 – 1.51 (m, 4H), 1.48 – 1.43 (m, 4H).,1.40 (d, *J* = 2.5 Hz, 18H), 1.38 – 1.07 (m, 12H). ESI-MS positive mode (methanol) m/z calc. $C_{45}H_{61}N_4O_6S_2$ calc. 817.4; found 817.3, $[M+H^+]^+$.

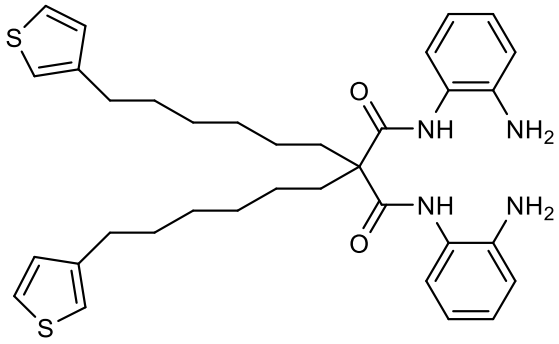

N1,N3-bis(2-aminophenyl)-2,2-bis(6-(thiophen-3-yl)hexyl)malonamide (**7**): **5** (90 mg, 0.11 mmol) was dissolved in dichloromethane (30 mL) and TFA (210 µL, 2.75 mmol) was added. The mixture was stirred for 24 h at room temperature. To the obtained solution an equimolar amount of saturated aqueous $NaHCO_3$ solution was added and the organic layer was separated and dried over $MgSO_4$ to yield an off-white honey-like oil (67 mg, 99%). ^{1}H NMR (300 MHz, DMSO-d_6) δ 9.39 (s, 2H), 7.41 (dd, *J* = 5.2, 2.7 Hz, 2H), 7.21 – 7.04 (m, 2H), 7.00 – 6.91 (m, 6H), 6.80 – 6.69 (m, 2H), 6.55 (t, *J* = 7.5 Hz, 2H), 4.51 – 5.04 (m, 4H), 2.49-2.66 (m, 4H), 2.07 – 1.93 (m, 4H), 1.67 – 1.49 (m, 4H), 1.38 – 1.13 (m, 12H). ESI-MS positive mode (methanol) m/z $C_{35}H_{45}N_4O_2S_2$ calc. 617.3; found 617.3, $[M+H^+]^+$.

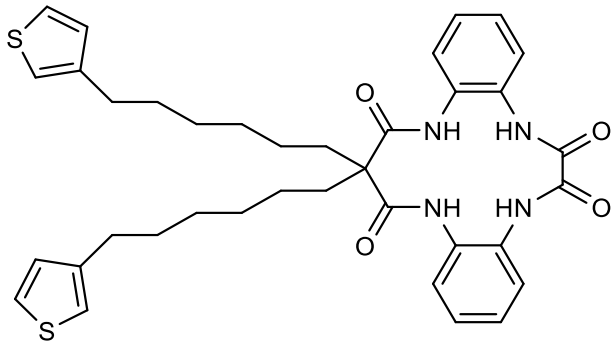

15,15-bis(6-(thiophen-3-yl)hexyl)-8,13-dihydro-5H-dibenzo[b,h][1,4,7,10] tetraazacyclotridecine-6,7,14,16(15H,17H)-tetraone (**H_4L**): A two-necked Schlenk flask equipped with a magnetic stirrer and a dropping funnel was heated to 160°C for 4 h. **7** (610 mg, 0.99 mmol) was dissolved in dry THF (50 mL) and NEt_3 (414µL, 3 mmol, 3 eq.) was added to the solution under Argon. The solution was added to the Schlenk flask through a rubber septum and was stirred at room temperature. A solution of oxalyl chloride (544 µL, 2 M in CH_2Cl_2) was diluted in dry THF (10 mL) and added to the dropping funnel through a septum under Argon. The drop rate was adjusted to one drop every five seconds. After 12 h stirring, a white precipitate ($[HN(C_2H_5)_3]^+Cl^-$) was formed and filtered off. The solvent was removed in vacuum to yield an off-white solid, which was recrystallized in a boiling hexane/dichloromethane (1:1) mixture to yield an off-white solid. The solid was thoroughly washed with methanol and water and dried in vacuum. (122mg, yield: 20 %)· ^{1}H NMR (300 MHz, DMSO-d_6) δ 9.50 (s, 2H), 9.46 (s, 2H), 7.69 (d, *J* = 7.8 Hz, 2H), 7.42 (dd, *J* = 4.9, 2.9 Hz, 2H), 7.37 – 7.25 (m, 6H), 7.11 (dd, *J* = 2.9, 1.3 Hz, 2H), 6.96 (dd, *J* = 4.9, 1.3 Hz, 2H), 2.57 (m, 4H), 1.96 (m, 4H), 1.59 (d, *J* = 8.6 Hz, 4H), 1.48 – 1.19 (m, 12H). ^{13}C NMR (101 MHz, DMSO-d_6) δ 172.43, 162.09, 143.04, 132.19, 130.49, 128.76, 127.98, 127.18, 126.38, 126.13, 125.29, 120.62, 59.64, 31.78, 30.38, 30.00, 29.57, 28.88, 23.82. ESI-MS negative mode (acetonitrile) m/z $C_{37}H_{42}N_4O_4S_2$ calc. 669.3; found 669.1 $[M\text{-}H^+]^-$, $C_{39}H_{42}F_3N_4O_6S_2$ calc. 783.3; found 783.1 $[M+F_3CCOO^-]^-$. Anal. Calcd for $C_{38}H_{48}N_4O_6S_2$: C, 63.31; H, 6.71; N, 7.77; S, 8.89. Found: C, 63.45; H, 6.56; N, 7.28, S, 8.84.

Synthesis of $[LCu]^{2-}$ and $[LCu]^{-}$ complexes.

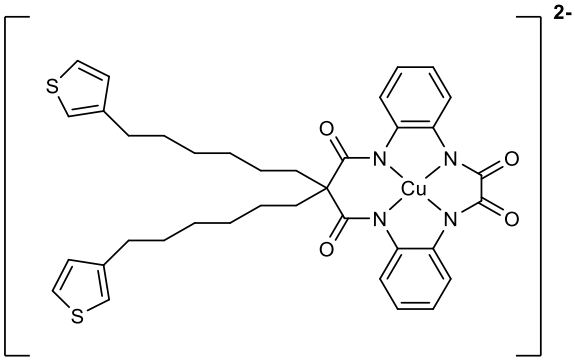

Synthesis of 15,15-bis(6-(thiophen-3-yl)hexyl)-8,13-dihydro-5H-dibenzo[b,h][1,4,7,10] tetraazacyclotridecine-6,7,14,16(15H,17H)-tetraone cuprate **$[LCu]^{2-}$**: **H_4L** (15 mg ,22.4 µmol) was suspended in methanol (10 mL) and $(Me_4N)OH$ (40 µL, 25 % in methanol , 89.6 µmol) was added under an Argon atmosphere. The suspension was heated to 50 °C until complete dissolution. Then, $Cu(OTf)_2$ (8 mg , 22.4 µmol) in methanol (2 mL) was added dropwise to the solution. After heating the mixture at 50 °C for 16 h, the solvent was removed in vacuum to obtained a brown residue. Afterwards, it was dissolved in acetonitrile (10mL) and settle it for 1h to obtain a white precipitate which was discarded after filtration through a glass frit. Filtrated obtained was evaporated to dryness to afford the product as a brown powder (17.7 mg, 70%). ESI-MS negative mode (methanol) m/z $C_{37}H_{38}CuN_4O_4S_2$ calc.: 729.2; found 729.0; $[M]^-$. Anal. Calcd. for $C_{37}H_{50}N_4O_{10}S_2$: C, 52.91; H, 6.93; N, 7.53; S, 6.89. Found: C, 53.00; H, 6.44; N, 7.42; S, 7.21.

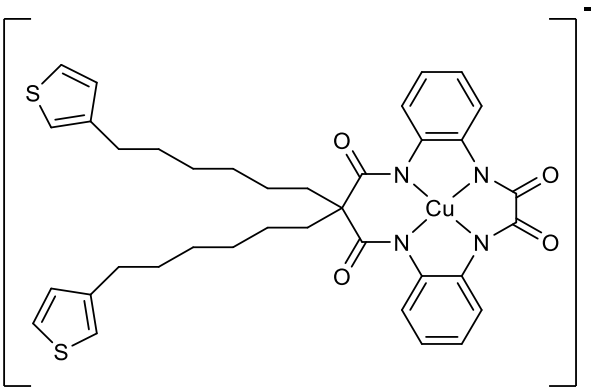

Synthesis of 15,15-bis(6-(thiophen-3-yl)hexyl)-8,13-dihydro-5H-dibenzo[b,h][1,4,7,10] tetraazacyclotridecine-6,7,14,16(15H,17H)-tetraone cuprate **$[LCu]^{-}$**: **$[LCu]^{2-}$** (10 mg , 11.4 µmol) was dissolved in dry MeOH (2.5 mL) and I_2 (25 mg, 0.2 mmol) was added to it. The resulting solution was heated up to 50 ^oC for 20 min. Afterwards, the cloudy solution was filtered through a glass frit and the obtained filtrate was evaporated to dryness. Resulting brown residue was washed with Et2O and dried under vacuum to afford **$[LCu]^{-}$** as dark brown powder (9.5 mg, 84%). ^1H NMR (500 MHz, CD_3 OD) δ 8.48 (dd, *J* = 8.1, 1.5 Hz, 2H), 8.09 (dd, *J* = 7.7, 1.7 Hz, 2H), 7.22 (dd, *J* = 4.9, 2.9 Hz, 2H), 6.99-6.91 (m, 4H), 6.90-6.87 (m, 2H), δ 6.87 (dd, *J* = 4.9, 1.3 Hz, 2H), 2.56 (t, *J* = 7.6, 4H), 1.97 – 1.92 (m, 4H), 1.58 – 1.53 (m, 4H), 1.03 –0.87 (m, 12H). ESI-MS positive mode (methanol) m/z $C_{37}H_{38}CuN_4O_4S_2$ calc.: 729.2; found 729.4; $[M]^+$

Preparation of molecular electroanodes

GC/CNT@p-[LCu]$^{2-}$. Preparation of **GC/CNT@p-[LCu]$^{2-}$** was performed in two separate steps. Firstly, a glassy carbon disk (GC, S = 0.078 cm^2) was functionalized with CNTs. For this purpose, a 1 mg·mL^{-1} CNT suspension was prepared and sonicated for 30 minutes. Afterwards, 80 µL of the solution were drop casted on a GC (4 x 20 µL), obtaining GC/CNT working electrode.[7] Afterwards, an acetonitrile solution of **[LCu]$^{2-}$** (3 mM) containing NH_4TfO (0.05 M) and *n*-Bu_4NPF_6 (0.05 M) as supporting electrolyte was used for the polymerization step. Electropolymerization was achieved by sequential CVs (50 cycles, v = 50 mV s^{-1}) in a range of potential from -0.7 V up to 0.6 V vs Fc^+/Fc, obtaining **GC/CNT@p-[LCu]$^{2-}$**. Γ = 7.3 nmol cm^{-2} of Cu (see Equation S3).

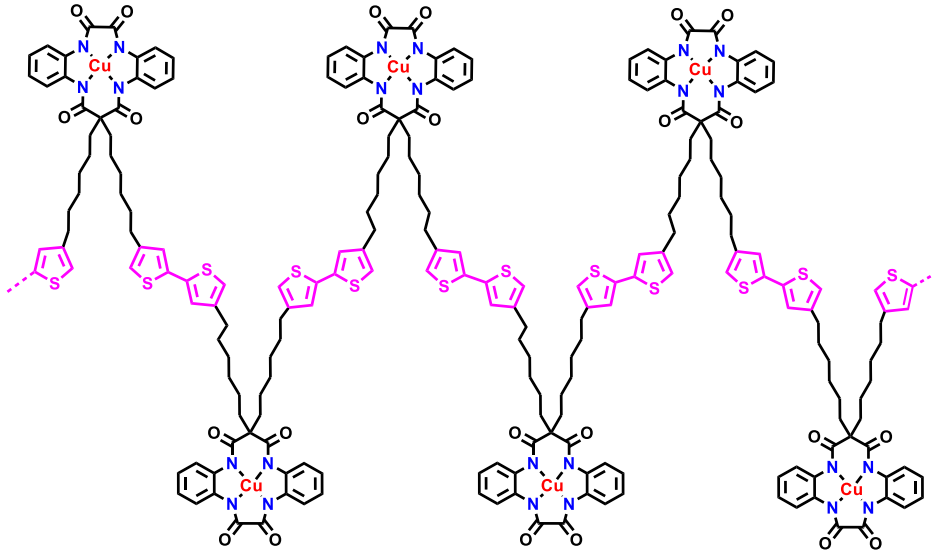

Structure of the thiophene substituted polymer obtained by anodic electropolymerization,

CP@p-[LCu]$^{2-}$ and **GF@p-[LCu]$^{2-}$.** The preparation of the electrodes was performed by using carbon paper (CP) or graphite felt (GF) without prior treatment. Acetonitrile solution of **[LCu]$^{2-}$** (3 mM) containing NH_4TfO (0.05 M) and *n*Bu_4PF_6 (0.05 M) as supporting electrolyte was used for the polymerization step. Electropolymerization was achieved by sequential CVs (50 cycles) in a range of potential from -0.7 V up to 0.6 V vs Fc^+/Fc.

Electroanodes for rotating ring disk electrode experiments

GC/CNT@p-[LCu]$^{2-}$. Preparation of **GC/CNT@p-[LCu]$^{2-}$** was performed in two separate steps. Firstly, the glassy carbon disk of the rotating ring disk electrode (GC, S = 0.126 cm^2) was functionalized with CNTs. For this purpose, a 1 mg·mL^{-1} CNT suspension was prepared and sonicated for 30 minutes. Afterwards, 100 µL (5 x 20 µL) of the solution were drop caster on a GC, obtaining GC/CNT working electrode.[7] Afterwards, an acetonitrile solution of **[LCu]$^{2-}$** (3 mM) containing NH_4TfO (0.05 M) and *n*-Bu_4NPF_6 (0.05 M) as supporting electrolyte was used for the polymerization step. Electropolymerization was achieved by sequential CVs (50 cycles, v = 50 mV s^{-1}) in a range of potential from -0.7 V up to 0.6 V vs Fc^+/Fc, obtaining **GC/CNT@p-[LCu]$^{2-}$**.

GC/RuO_2. Preparation of **GC/RuO_2** was performed by sonicating a 1 mg·mL^{-1} suspension of RuO_2 and drop casting (5 x 5 μL) the resulting suspension on the glassy carbon disk of the rotating ring disk electrode (GC, S = 0.126 cm^2).

Electroanodes for XAS analysis

GCp/CNT@p-[LCu]$^{2-}$. Preparation of **GCp/CNT@p-[LCu]$^{2-}$** was performed in two separate steps following a similar procedure. Firstly, a **GC_p** electrode (20 x 10 x 0.18 mm) was functionalized with CNTs. For this purpose, a 1 mg·mL^{-1} CNT suspension was prepared and sonicated for 30 minutes. Afterwards, 180 µL (6 x 30 µL, one site S = 1 cm^2) of the colloidal suspension were drop casted on a GC, obtaining **GCp/CNT** working electrodes. Afterwards, an acetonitrile solution of **[LCu]$^{2-}$** (3 mM) containing NH_4TfO (0.05 M) and *n*-Bu_4NPF_6 (0.05 M) as supporting electrolyte was used for the polymerization step. Electropolymerization was achieved by 25 sequential CVs in a range of potential from -0.7 V up to 0.6 V vs Fc^+/Fc, obtaining **GC/CNT@p-[LCu]$^{2-}$**, containing a mass deposition of Γ = 3.5 nmol cm^{-2} of Cu (see Equation S3).

The samples were then subjected to a controlled potential electrolysis at 1.3 V *vs*. NHE in pH 7 phosphate buffer for the corresponding time (0, 1, 2, 6 and 24 h). Charges of 0.814 C, 1.628 C, 3.053 C and 36.98 C were obtained from each bulk electrolysis experiments (1, 2, 6 and 24 h) respectively, achieving 60 (1h), 120 (2h) 300 (6h) and 2700 (24 h) turn-over numbers (TON). The monomeric complex powder samples were drop casted on a **GCp** as reference.

NMR Spectroscopy

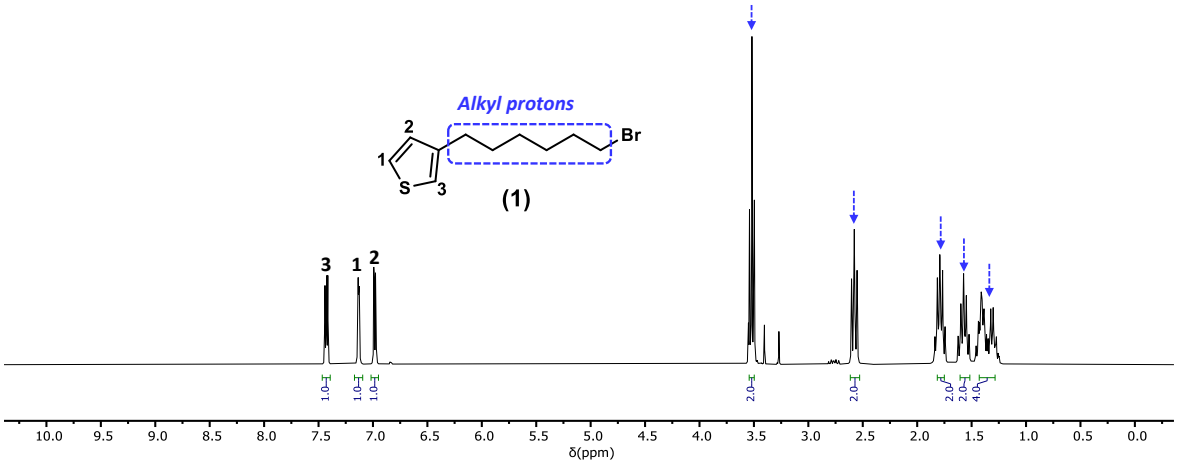

Figure S1. ^{1}H-NMR spectrum of **1** (300 MHz, 298 K, DMSO-d_6).

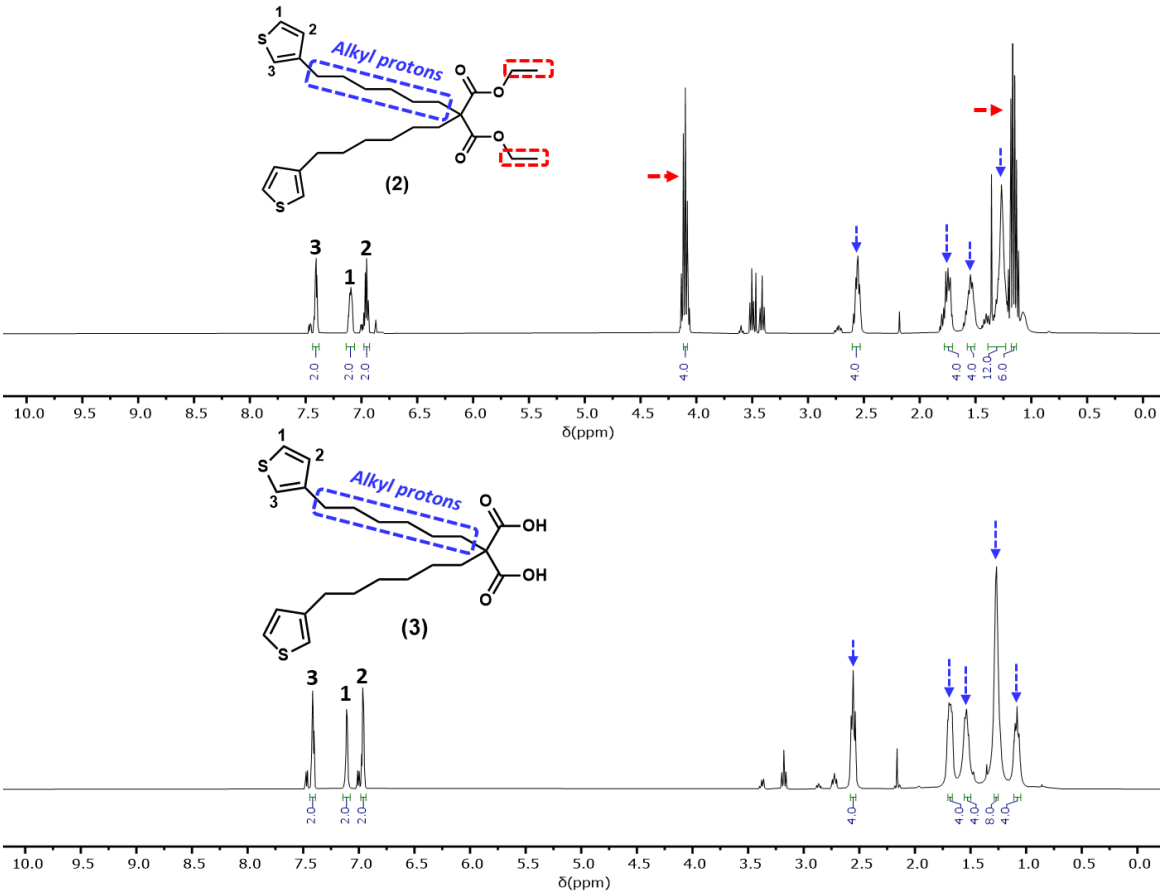

Figure S2. ^{1}H-NMR spectrum of **2** (top) and **3** (bottom) (300 MHz, 298 K, DMSO-d_6).

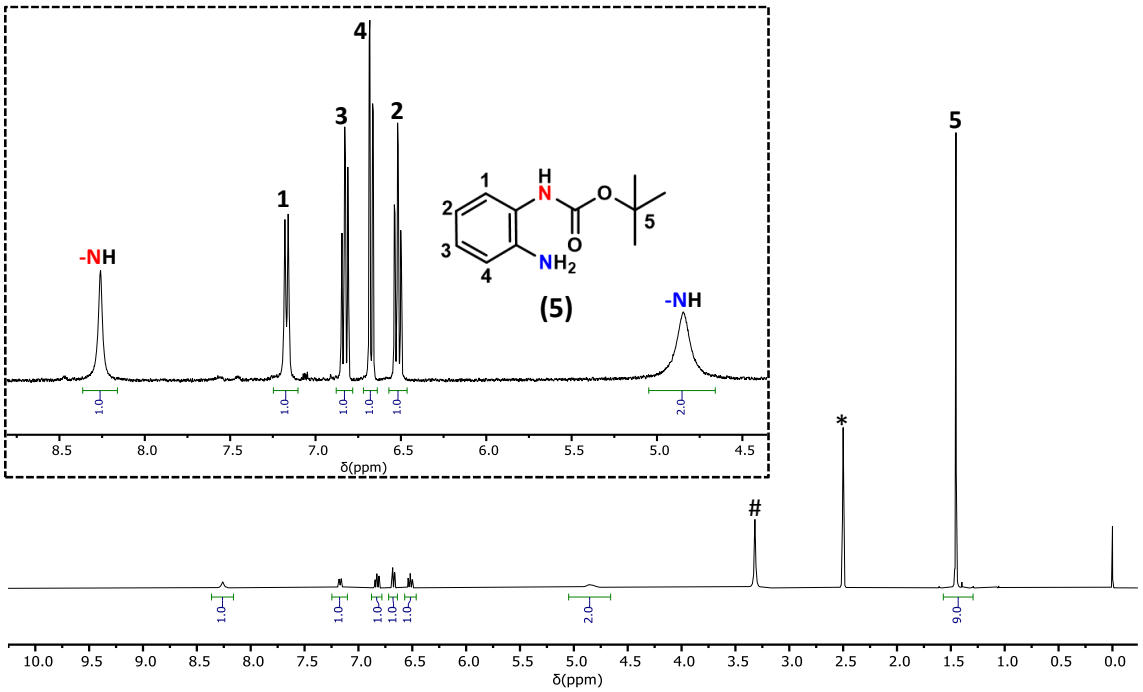

Figure S3. ^{1}H-NMR spectrum of **5** (300 MHz, 298 K, DMSO-d_6), *DMSO, $^{\#}H_2O$.

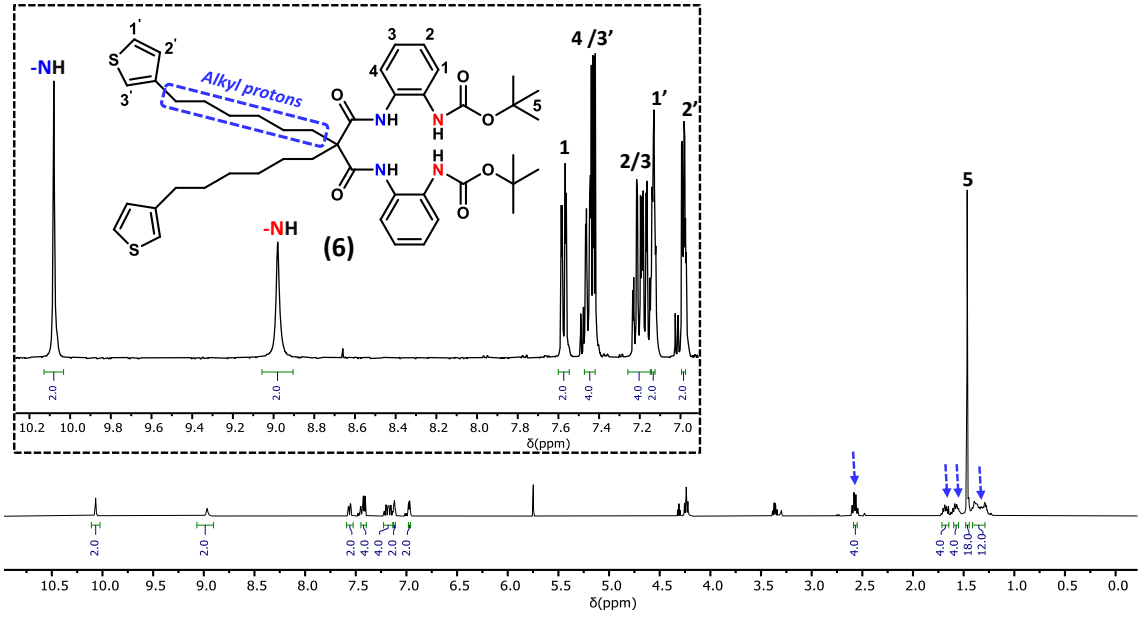

Figure S4. ^{1}H-NMR spectrum of **6** (300 MHz, 298 K, DMSO-d_6).

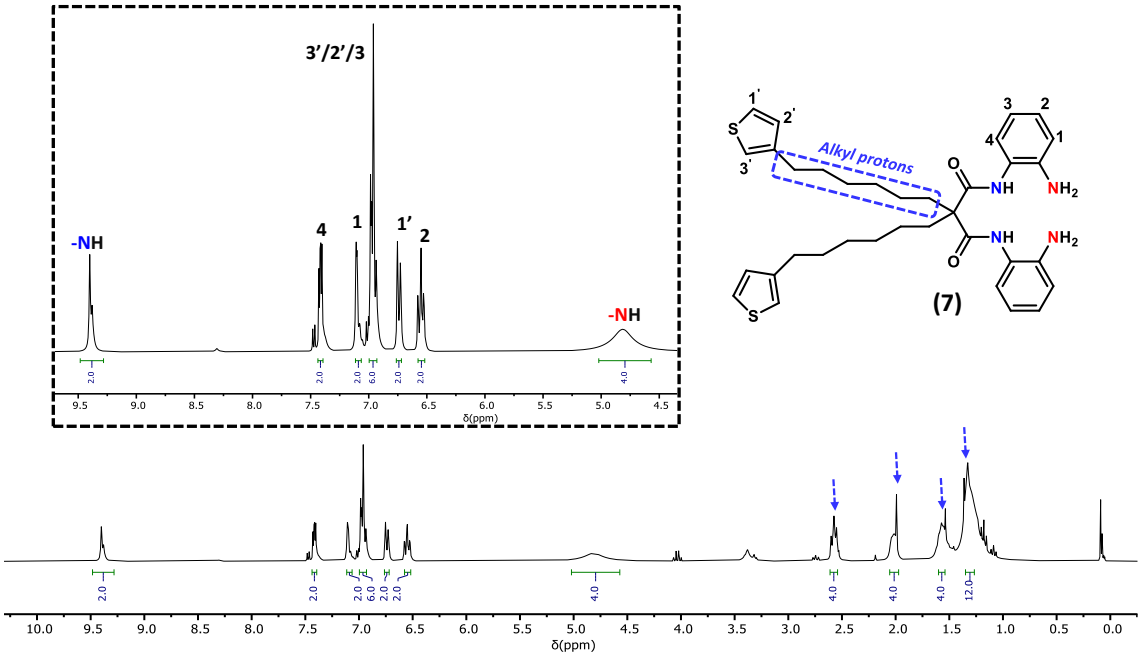

Figure S5. ^{1}H-NMR spectrum of **7** (300 MHz, 298 K, DMSO-d_6).

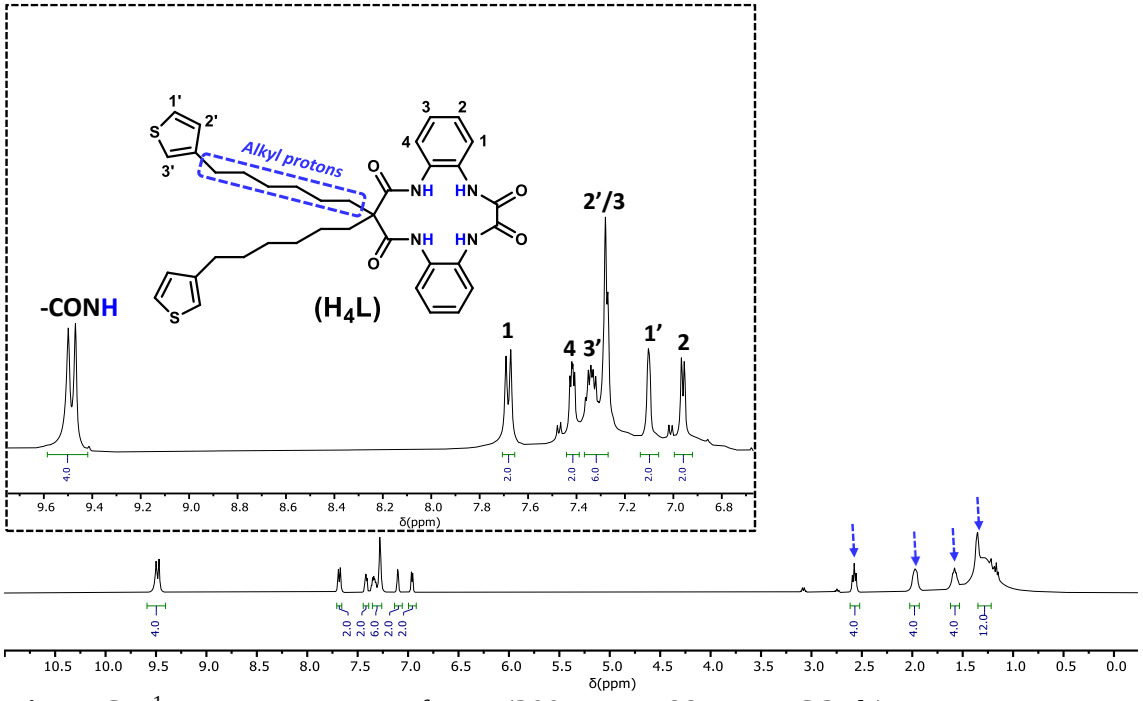

Figure S6. ^{1}H-NMR spectrum of **H_4L** (300 MHz, 298 K, DMSO-d_6).

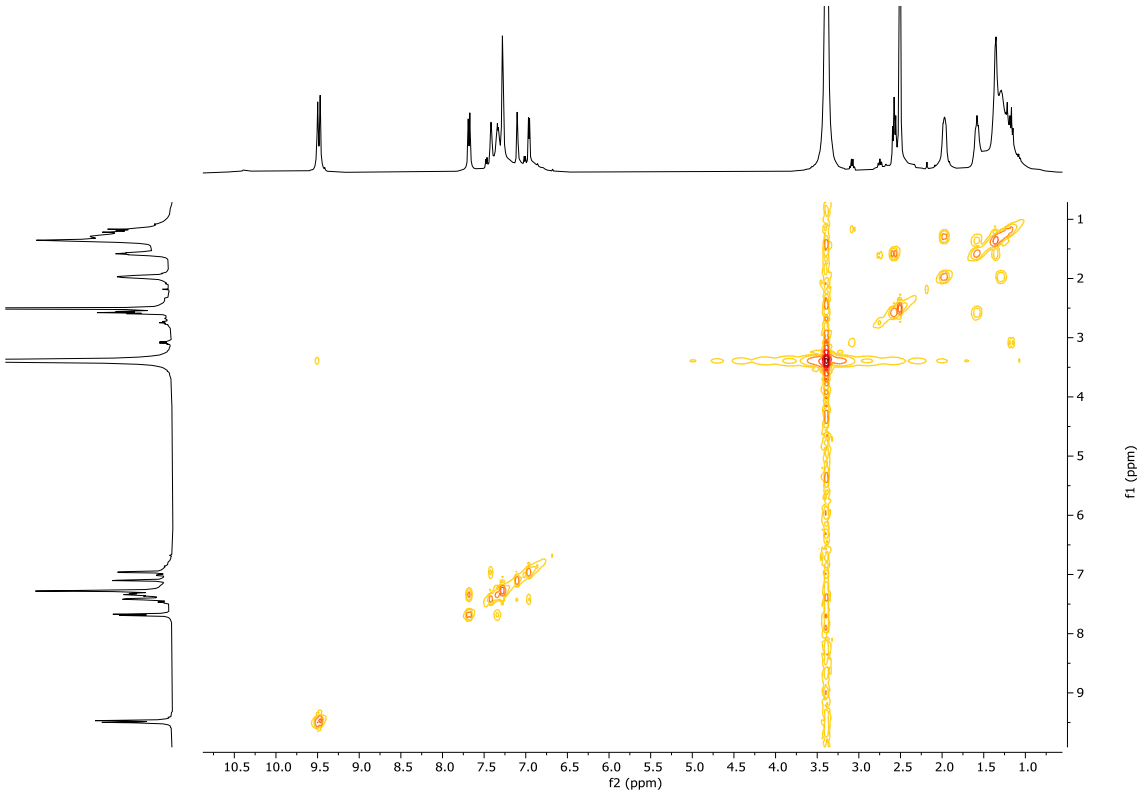

Figure S7. COSY spectrum of **H_4L** (500 MHz MHz, 298 K, DMSO-d_6).

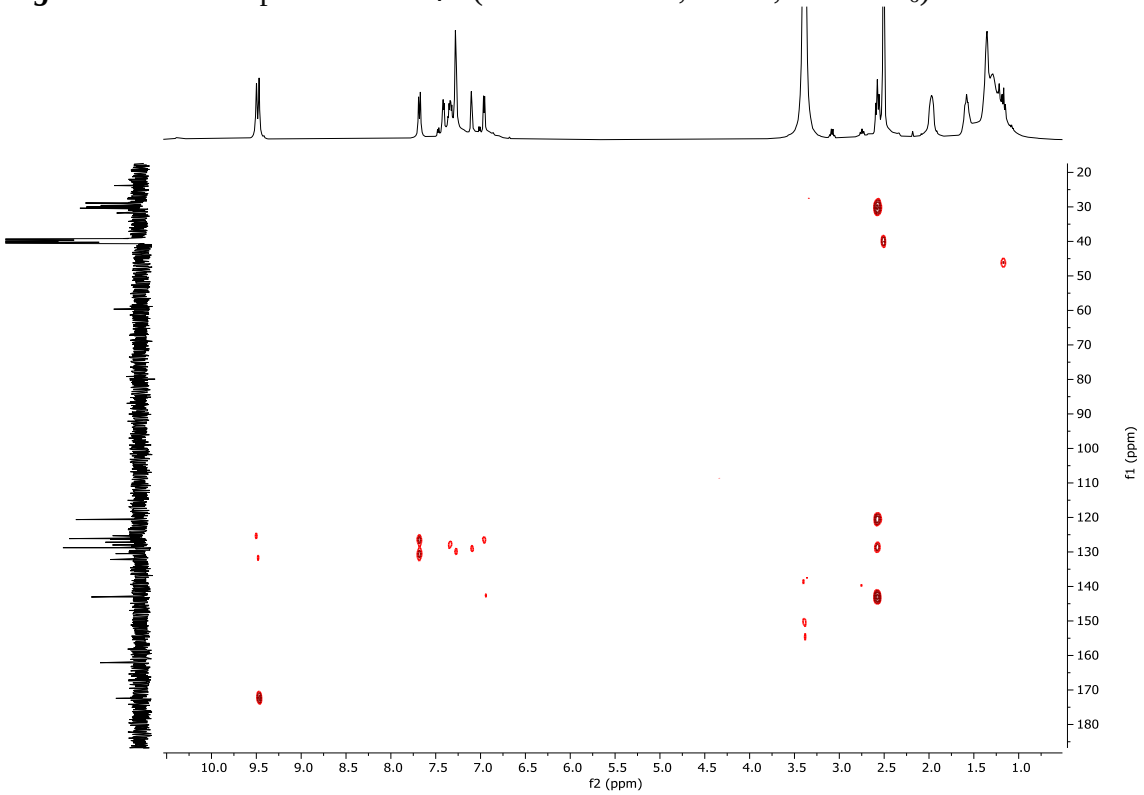

Figure S8. HSQC spectrum of **H_4L** (500 MHz, 298 K, DMSO-d_6).

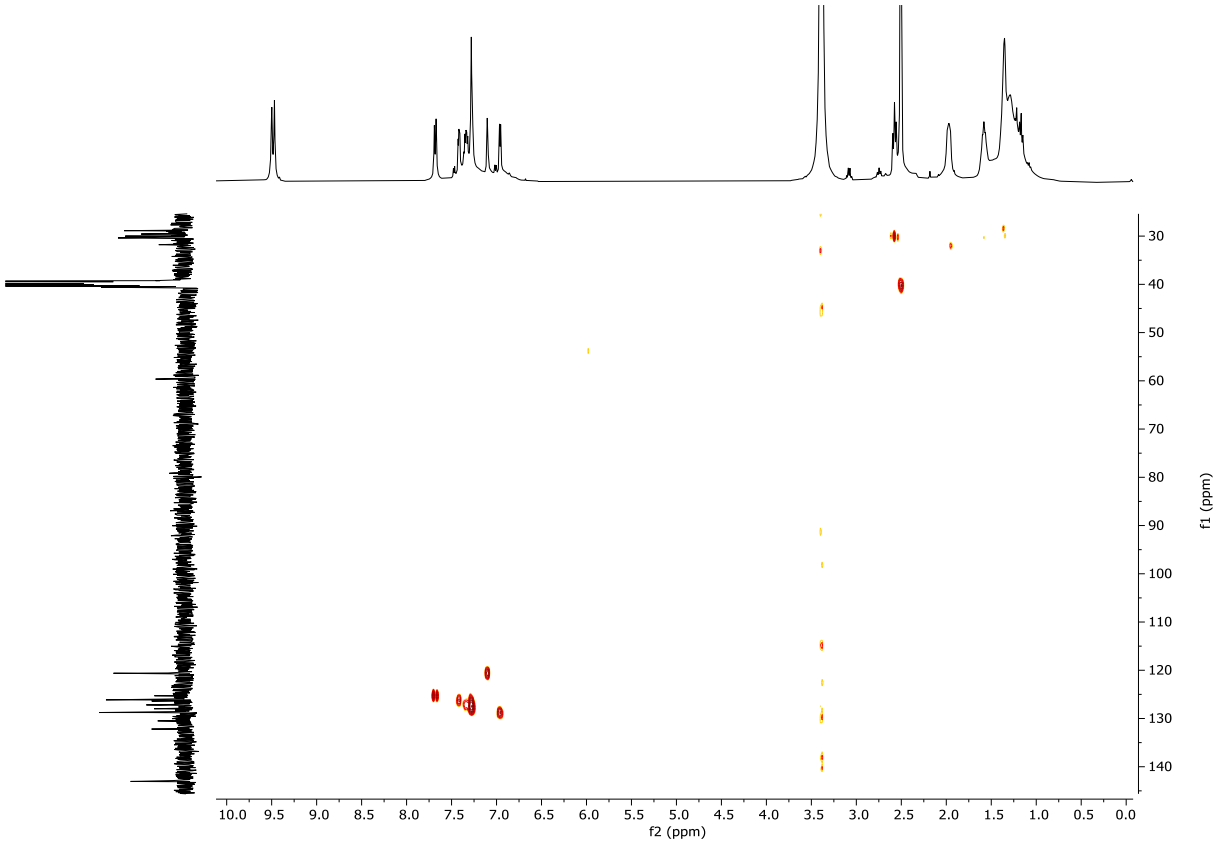

Figure S9. HMBC spectrum of **H_4L** (500 MHz, 298 K, DMSO-d_6).

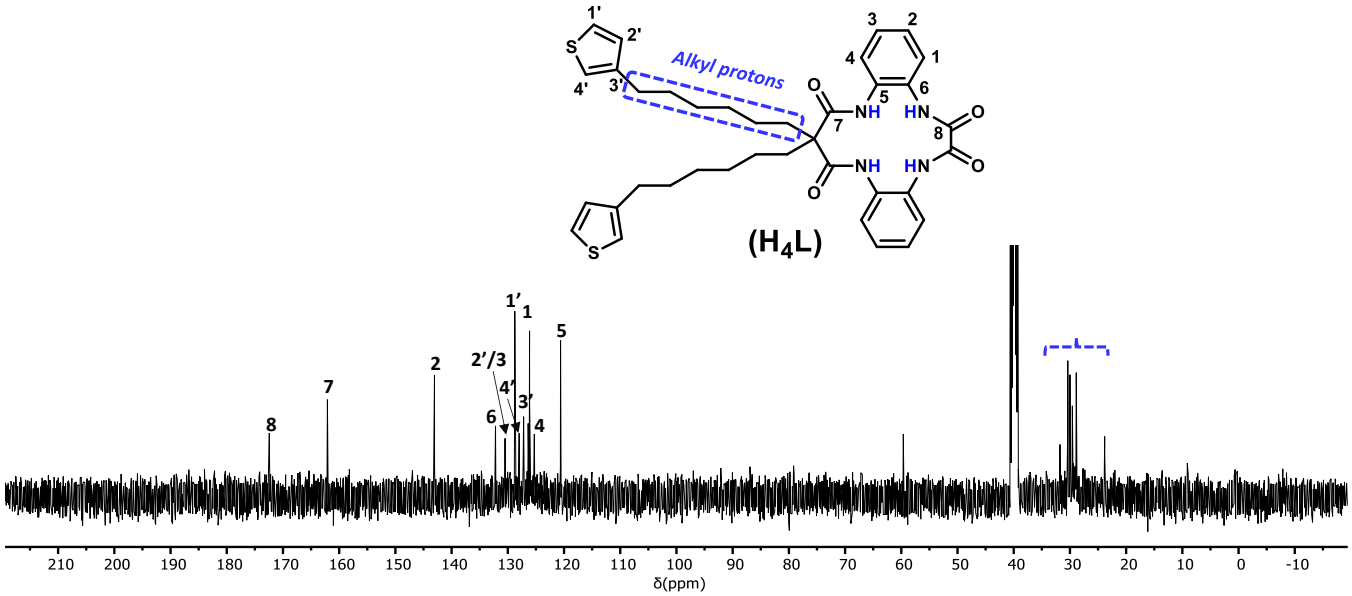

Figure S10. ^{13}C-NMR spectrum of **H_4L** (500 MHz, 298 K, DMSO-d_6).

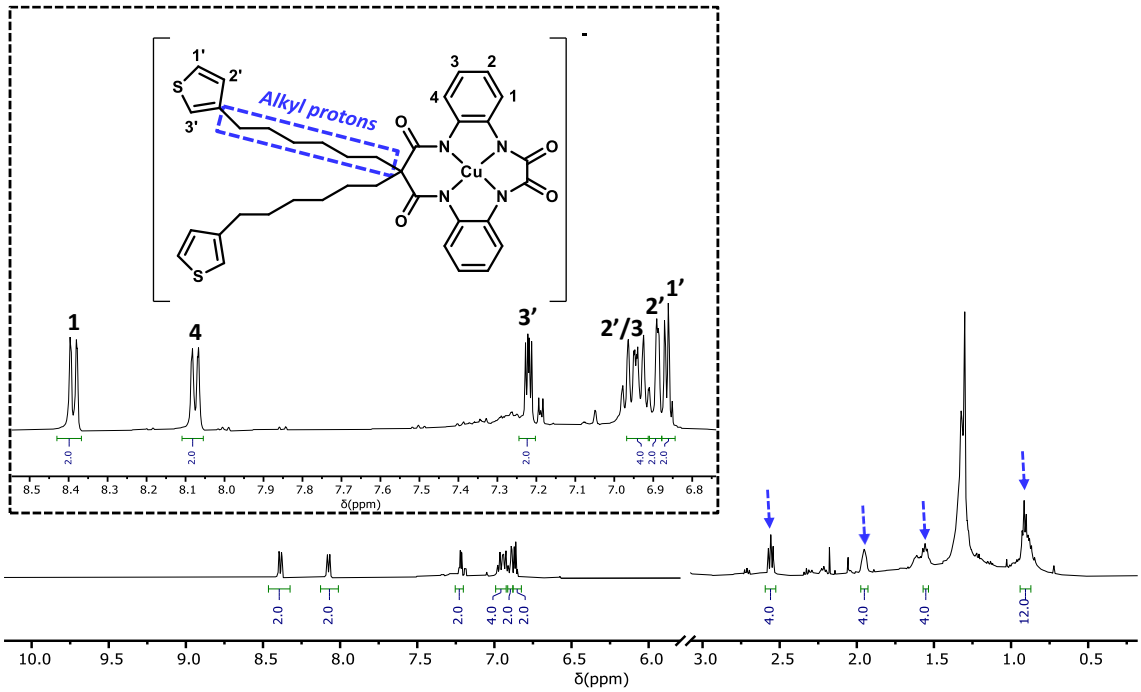

Figure S11. HNMR spectrum of **[LCu]**$^{-}$ (500 MHz, 298 K, MeOH-d_4).

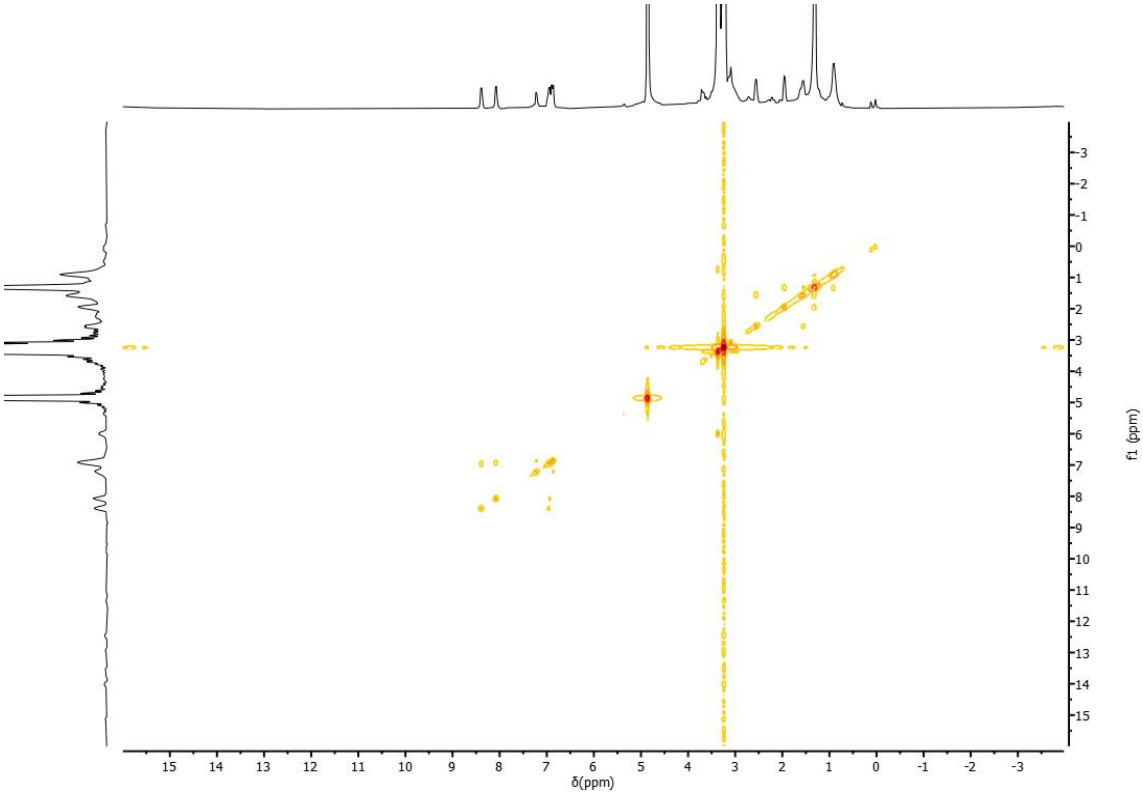

Figure S12**:** COSY spectrum of **[LCu]**$^{-}$ (500 MHz MHz, 298 K, MeOH-d_4).

Mass spectrometry

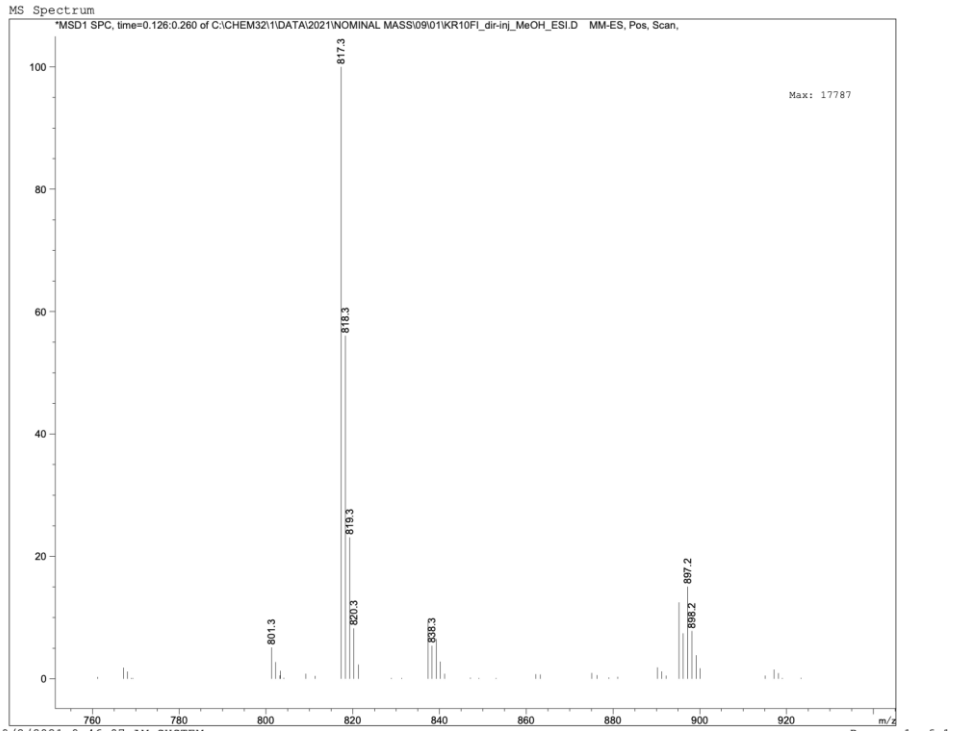

Figure S13. (+)-ESI-MS spectrum for **6** Calc. for [M+H$^+$], ($C_{45}H_{61}N_4O_6S_2$): 817.4, found 817.3.

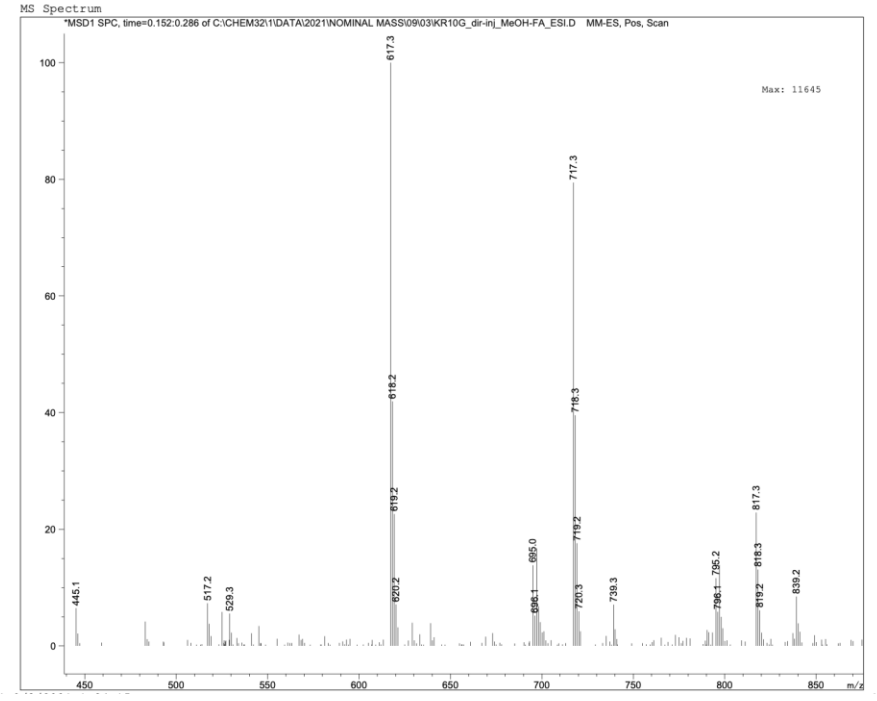

Figure S14. (+)-ESI-MS spectrum for **7** Calc. for [M+H$^+$], ($C_{35}H_{45}N_4O_2S_2$): 617.3, found 617.3.

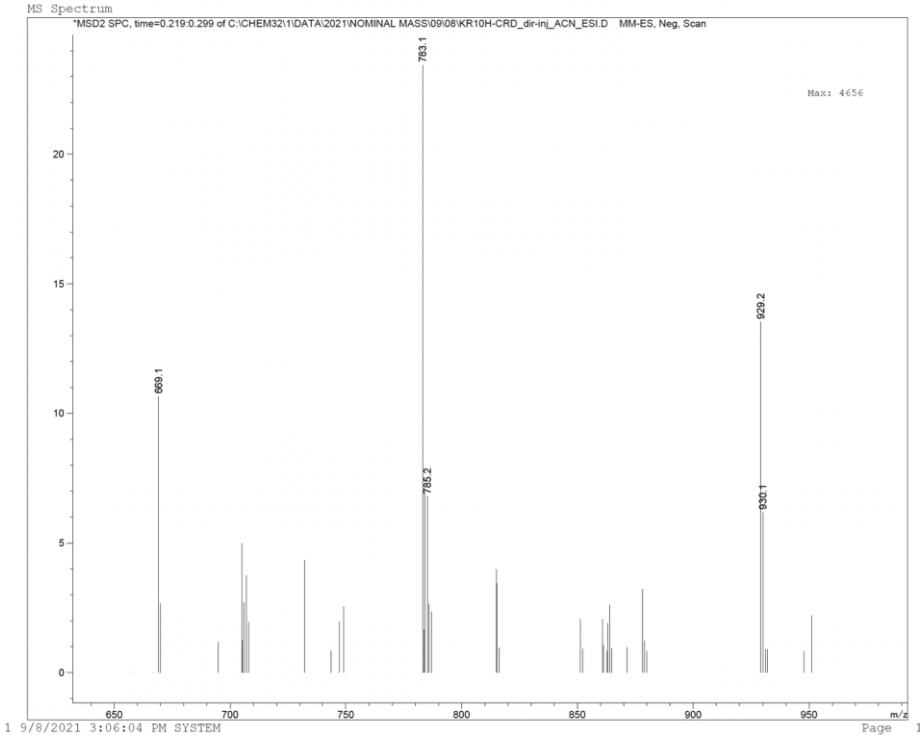

Figure S15. (-)-ESI-MS spectrum for **H_4L**. Calc. for $[M\text{-}H^+]^-$, ($C_{37}H_{41}N_4O_4S_2$): 669.3, found 669.1; for $[M+F_3CCOO^-]^-$, $C_{39}H_{42}F_3N_4O_6S_2$ calc. 783.3; found 783.1.

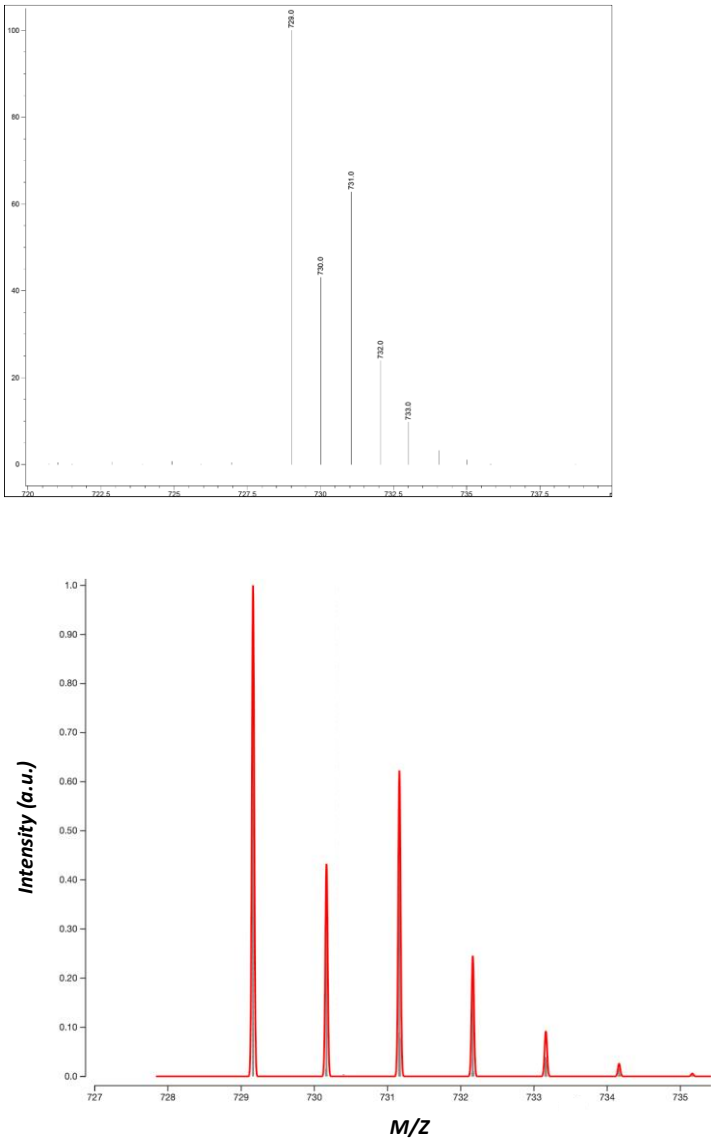

Figure S16. (-)-ESI-MS spectrum (top) and simulated isotopic pattern (bottom) $[\mathbf{LCu}]^{2-}$ Calc. for $[M]^-$, ($C_{37}H_{38}CuN_4O_4S_2$): 729.2; found 729.0.

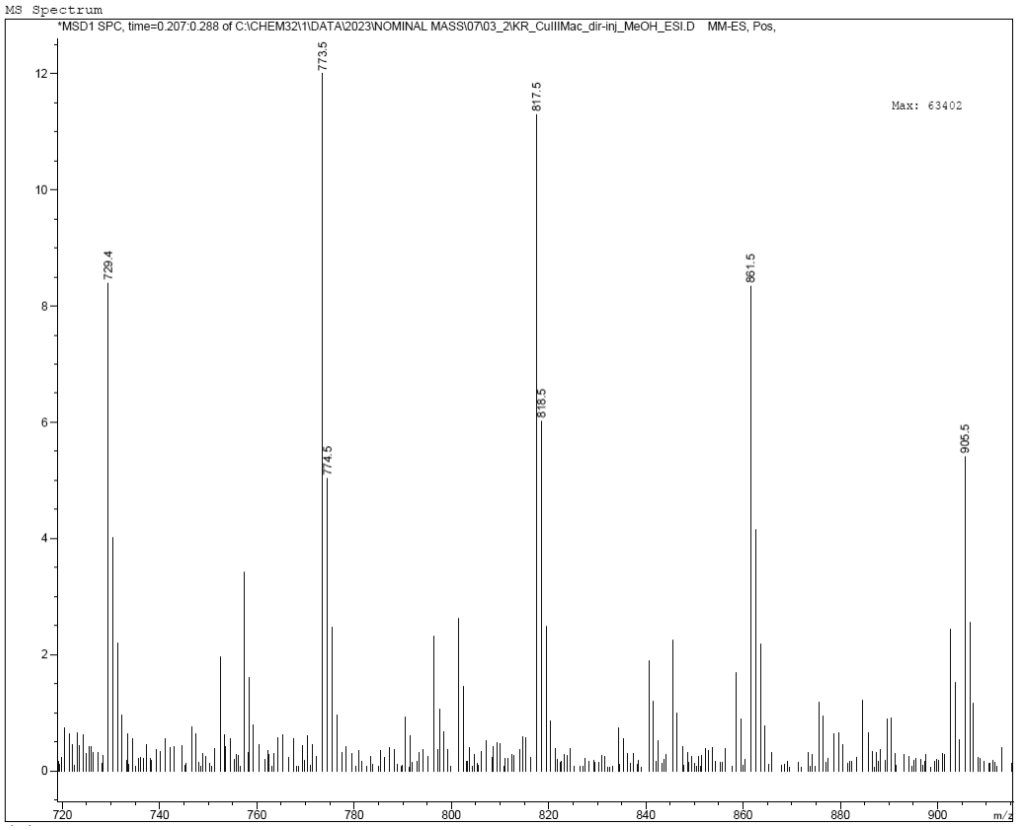

Figure S17. (+)-ESI-MS spectrum for **[LCu]**$^{-}$. Calc. for $[M]^{+}$, ($C_{37}H_{38}CuN_4O_4S_2$): 729.2; found 729.4.

UV-vis and ATR-IR spectroscopy

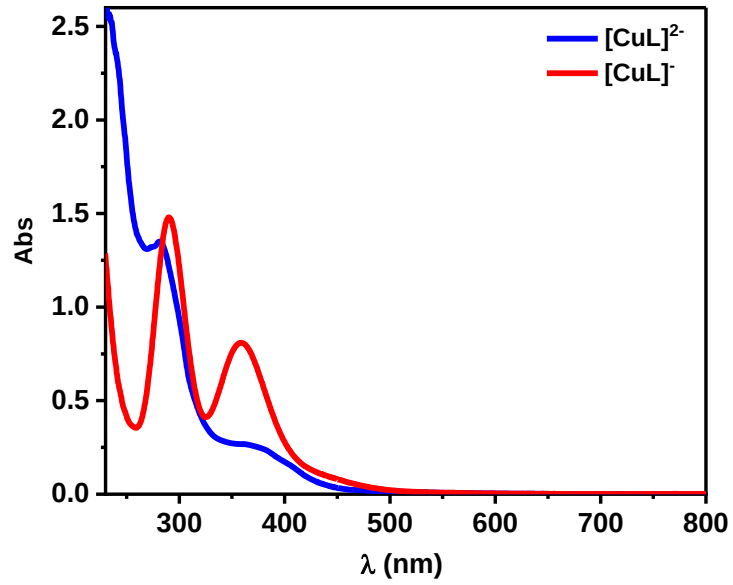

Figure S17b. UV-vis absorption spectra of 1 mM solutions of **[LCu^{II}]$^{2-}$** and **[LCu^{III}]$^{-}$** in MeOH.

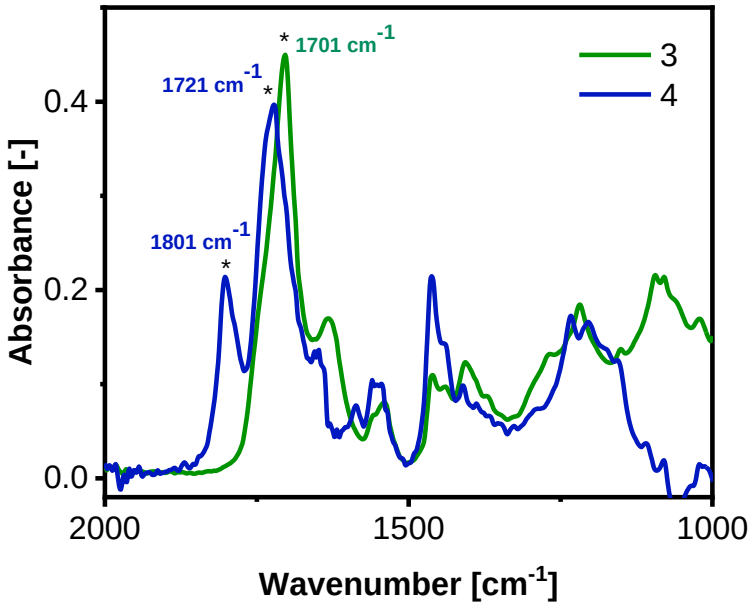

Figure S18. ATR-IR spectrum of **3** and **4**

Electrochemical measurements

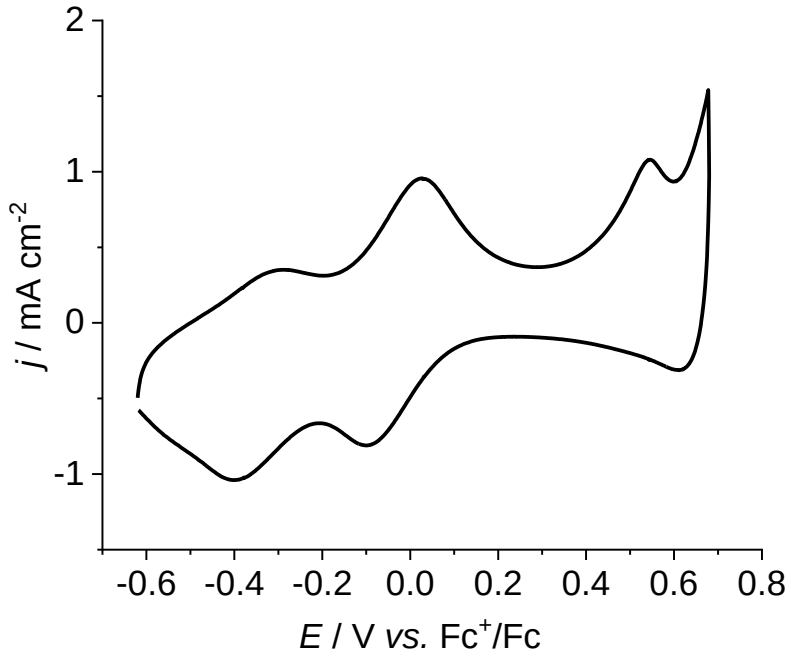

Figure S19. Cyclic voltammetry of **GC/CNT@p-[LCu]$^{2-}$** (Γ = 6.4 nmol cm^{-2}) in a clean acetonitrile solution containing a mixture of 0.05 M nBu_4PF_6 and 0.05 NH_4OTf as supporting electrolyte at a scan rate of 50 mV s^{-1}.

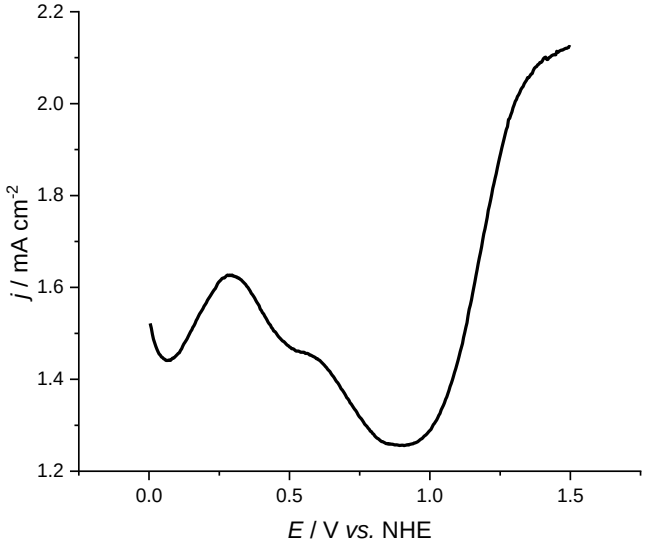

Figure S20. DPV of **GC/CNT@p-[LCu]$^{2-}$** (Γ = 6.4 nmol cm^{-2}) in an aqueous phosphate buffer (0.1 M) solution at pH 7.1.

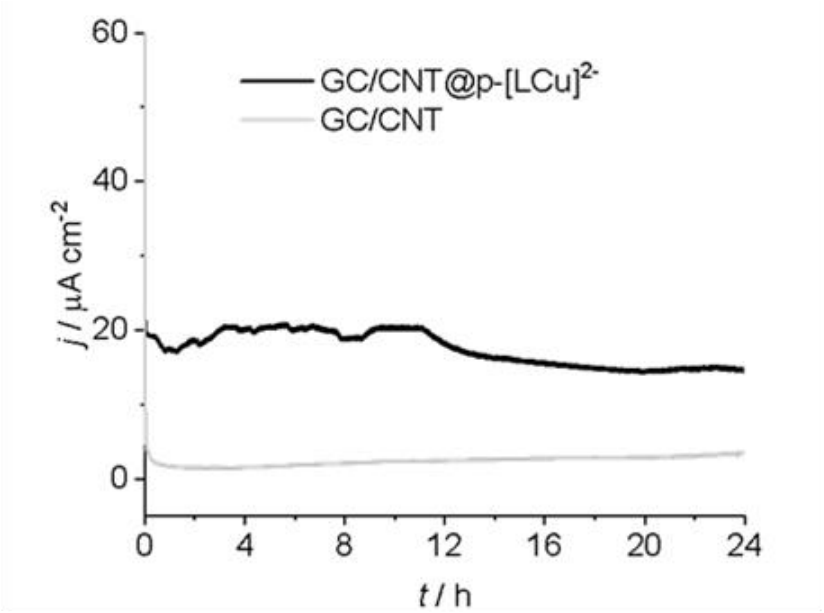

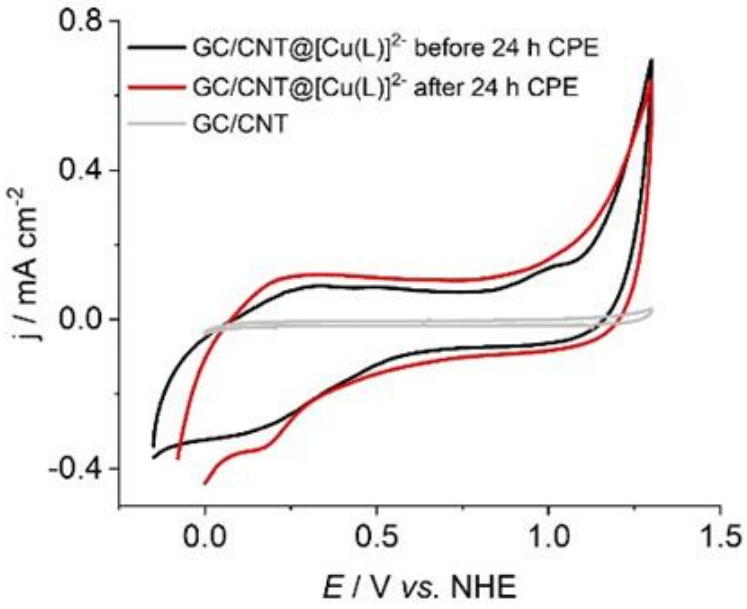

Figure S21. (**Top**) CPE experiment with **GC/CNT@p-[LCu]$^{2-}$** (Γ = 6.4 nmol cm^{-2}) (black line) and **GC/CNT** (gray line) as blank in an aqueous pH 7 phosphate buffer (0.1 M) solution at an applied potential of 1.3 V vs. NHE for 24 h. Charge, 1.48 C -> 1.52x10^{-5} mmols of O_2 (assuming 100% Faradaic efficiency and 4 e- per O_2 molecule). Loading, 6.4 (nmols/cm^2) x 0.078 (cm^2) = 0.50 nmols of Cu. TON = 600 per Cu complex. (**Bottom**) CV of **GC/CNT@p-[LCu]$^{2-}$** (Γ = 6.4 nmols/cm^2) before and after the CPE experiment in an aqueous phosphate buffer (0.1 M, pH 7) at a scan rate of 50 mV/s.

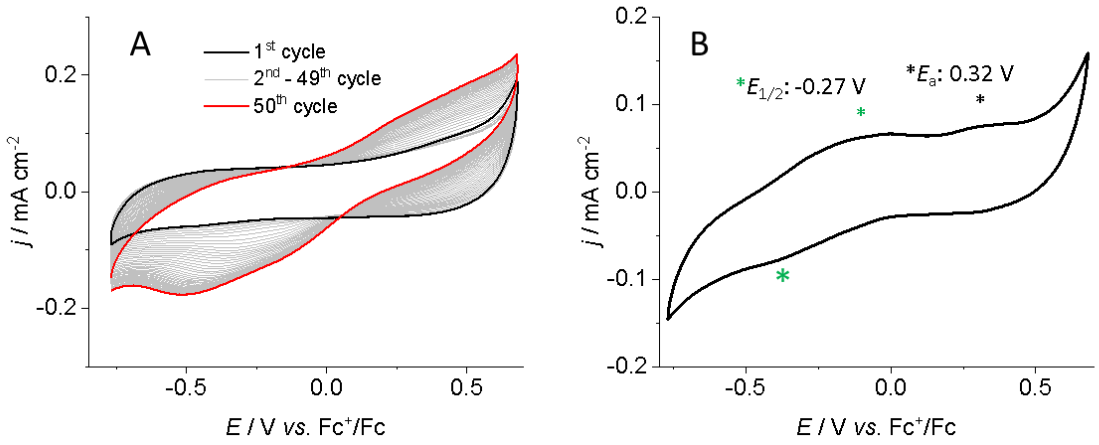

Figure S22. (**A**) 50 consecutive CV cycles (E_i = E_f = -0.7 V, E_c = 0.6 V) of a MeCN solution containing 3 mM of **H_4L** and a mixture of 0.05 M nBu_4PF_6 and 0.05 *M* NH_4TfO as supporting electrolyte at a scan rate of 50 mV s^{-1}, using a **GC/CNT** as a WE. (**B**) Cyclic voltammetry of the modified electrode, **CP@L_n**, immersed in an 0.1 M aqueous phosphate buffer solution at pH 7 upon cycling (E_i = E_f = -0.7 V, E_c = 0.6 V) at a scan rate of 50 mV s^{-1}.

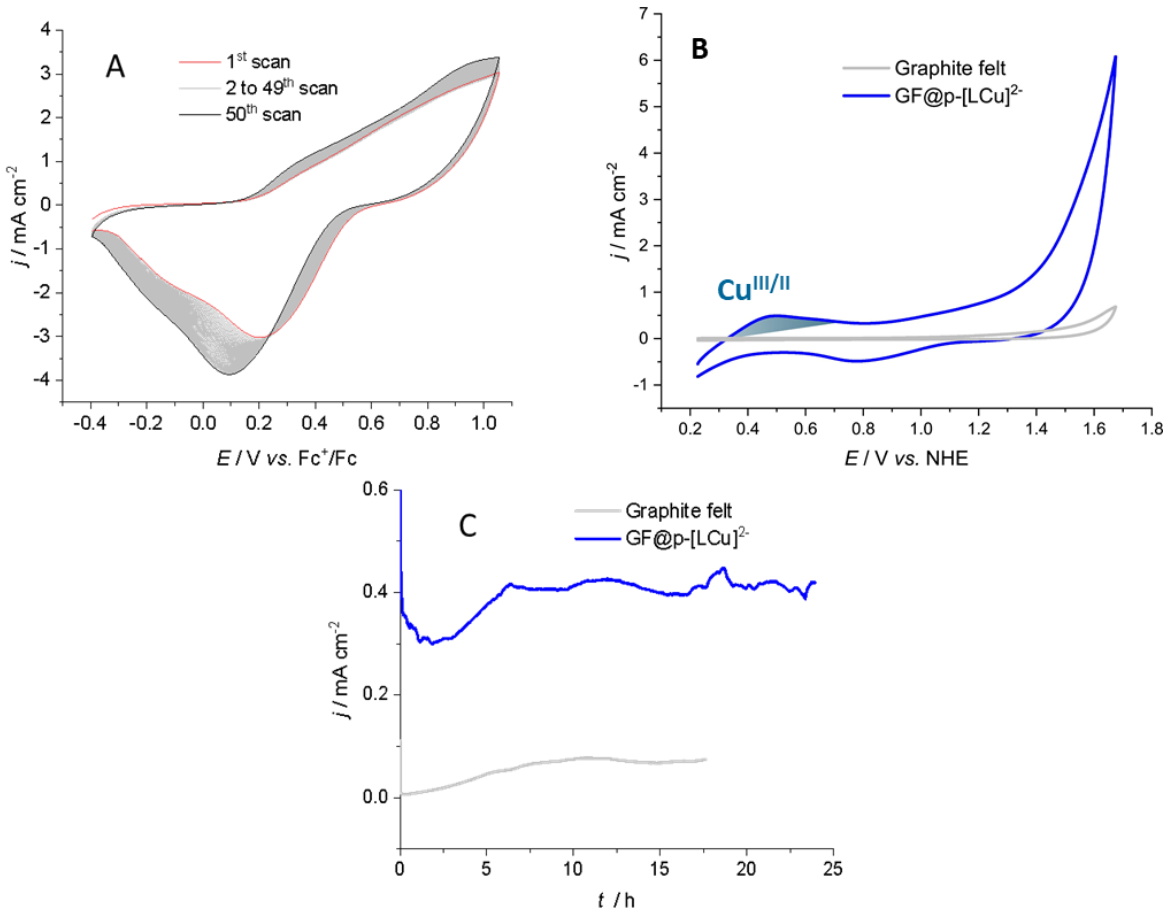

Figure S23. **A**, 50 consecutive CV cycles ($E_i = E_f$ = -0.4 V, E_c = 1 V) of a MeCN solution containing 3 mM of **[LCu]$^{2-}$** and a mixture of 0.05 M *n*-Bu_4NPF_6 and 0.05 M NH_4TfO as supporting electrolyte at a scan rate of 50 mV s^{-1}, using a **GF** as a WE. **B,** Cyclic voltammetry of the modified electrode, **GF@[LCu]$^{2-}$** (Γ = 6.8 nmol cm^{-2}; size = 1 cm^2), immersed in an 0.1 M aqueous phosphate buffer solution at pH 7 upon cycling ($E_i = E_f$ = 0.2 V, E_c = 1.7 V) at a scan rate of 50 mV s^{-1}. **C,** 24 h CPE experiment with **GF@[LCu]$^{2-}$** (Γ = 6.8 nmol cm^{-2}) (blue line) and 16 h **GF** (gray line) as blank in an aqueous pH 7 phosphate buffer (0.1 M) solution at an applied potential of 1.3 V *vs*. NHE. CPE of **GF** was recorded up to 16 h due to a degradation of the graphite felt during the experiment, obtaining a dark solution over time. The total charge produced during the 24 h CPE experiment was 30.05 C after subtraction of the current obtained from the blank. Assuming 100% of Faradaic efficiency and 4 e^- per O_2 molecule, we obtained 7.78x10^{-2} mmols of O_2 which represent 11200 TONs of oxygen produced per Cu center.

Rotating-ring disk electrode (RRDE) experiments

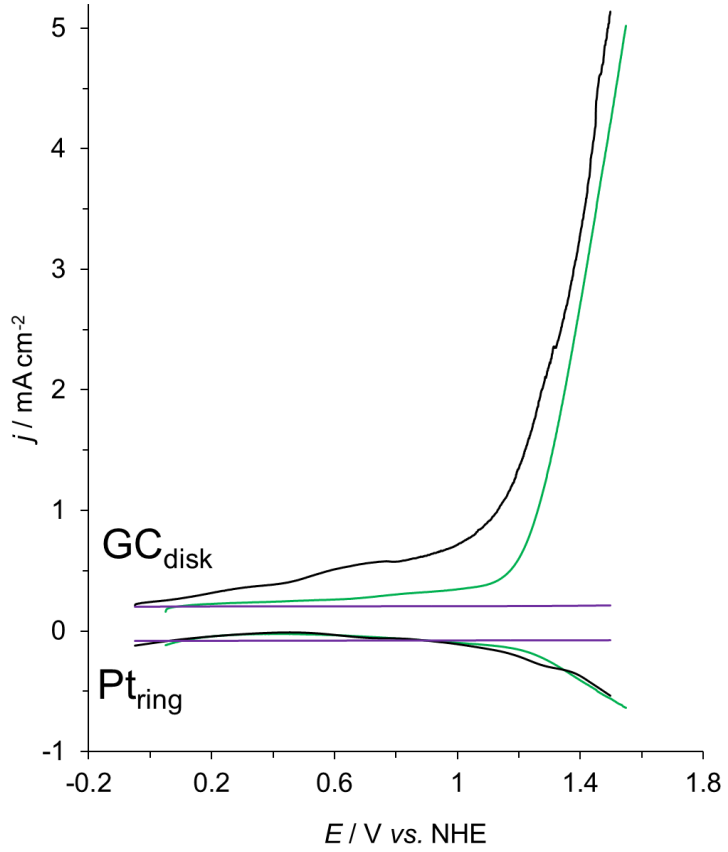

Figure S24. RDDE experiments using **GC/CNT@p-[LCu]$^{2-}$**(Γ = 0.3 nmol cm^{-2}) (black line), **GC/RuO$_2$** green line) and **GC/CNT** (purple line) as the inner working disk electrode (ϕ = 4 mm, S = 0.126 cm^2) in an aqueous pH 7 phosphate buffer (0.1 M) solution under nitrogen atmosphere and at 1600 rpm. *I* vs. *E* plot from the working electrode (top) and simultaneous oxygen reduction at Pt ring electrode (Pt ring: $\phi_{outer\text{-}Ring}$ = 7 mm, $\phi_{inner\text{-}Ring}$ = 5 mm) at E_{app} = -0.5 V *vs.* NHE (bottom). Assuming the RuO_2 gives 100% Faradaic efficiency the nearly overlapping plot for **GC/CNT@p-[LCu]$^{2-}$** implies also Faradaic efficiency very close to 100%.

Microscopy

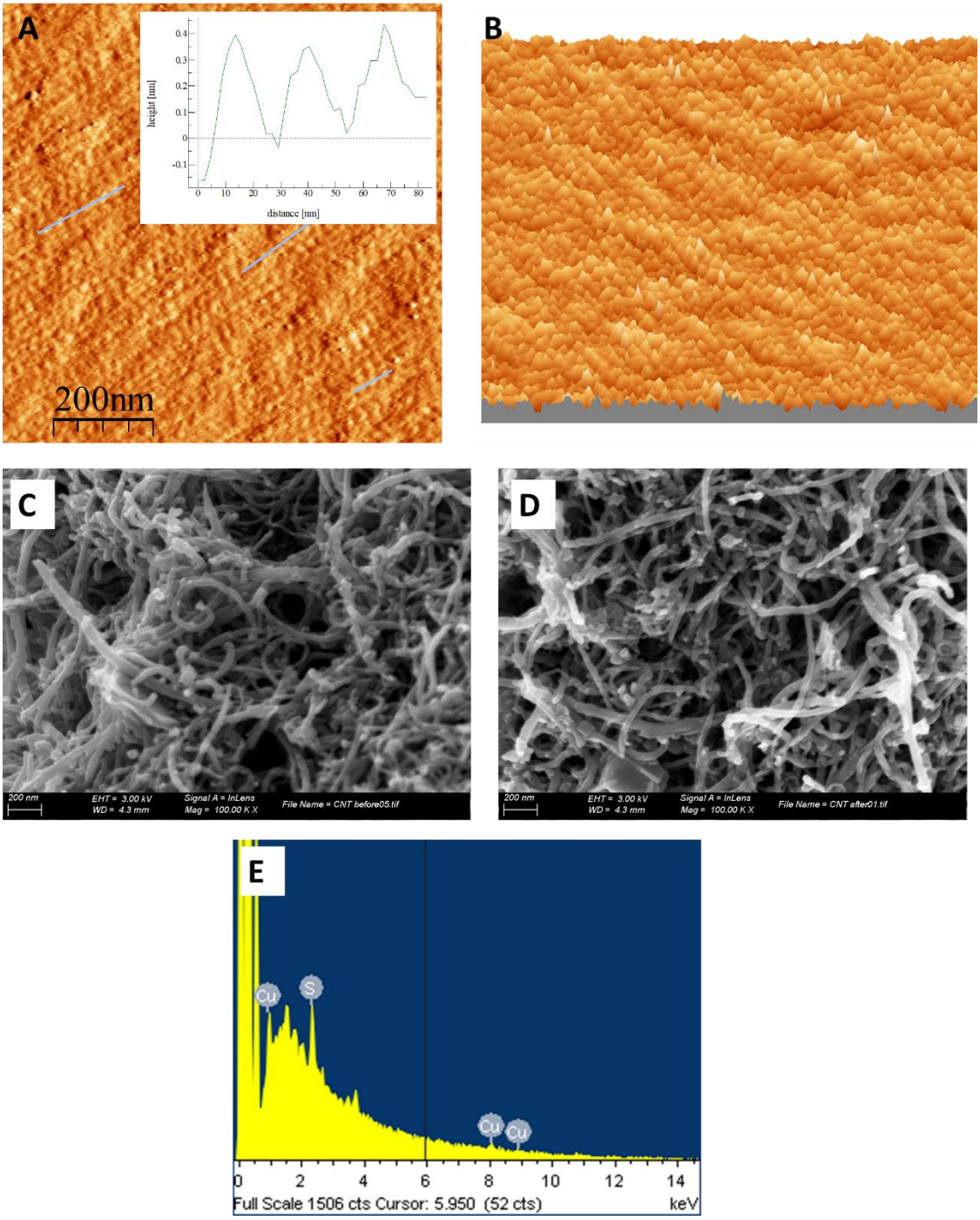

Figure S25. (***A***) AFM phase images of ***GC/CNT@p-[LCu]$^{2-}$***. (***B***) 3D surface pattern of the area shown in *A*. (***C***) SEM image of a ***GC/CNT@p-[LCu]$^{2-}$*** electrode. (***D***) SEM image of a ***GC/CNT@p-[LCu]$^{2-}$*** electrode after a CPE experiment in an aqueous pH 7 phosphate buffer (0.1 M) solution at an applied potential of 1.3 V vs. NHE for 6 h. (***E***) EDX spectrum of **GC/CNT@p-[LCu]$^{2-}$**showing the presence of **[LCu]$^{2-}$** on the CNTs.

X-ray absorption spectroscopy

Tab. S1. List of the scattering paths used for the fitting of the experimental spectra used as a base for fitting all the spectra. R_{eff} is half of the scattering path length, equal to the interatomic distance for SS paths.

Code	Path Scattering type		R_{eff} (Å)	Degeneracy
1	$Cu \rightarrow N$	SS	1.904	4
2	$Cu \rightarrow C1$	SS	2.762	4
3	$Cu \rightarrow C2$	SS	2.844	4
4	$Cu \rightarrow O$	SS	3.983	4
5	$Cu \rightarrow C1 \rightarrow N$	MS	3.035	8

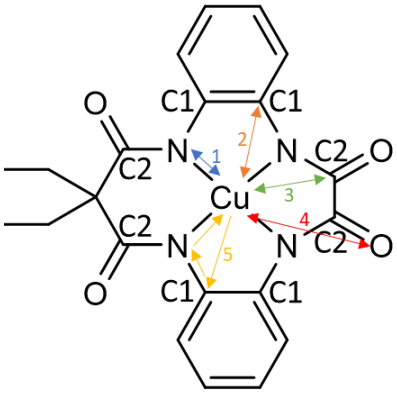

Figure S26. Geometry of **[(Mac)Cu]$^{2-}$** scattering paths used for fitting the EXAFS spectra.

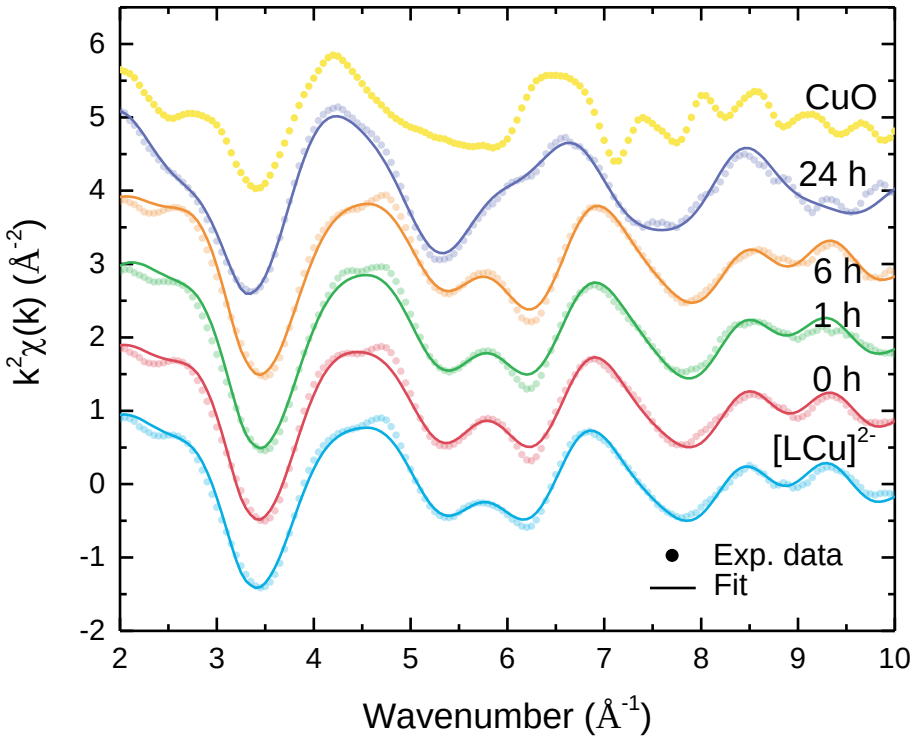

Figure S27. EXAFS signal recorded for **[LCu]$^{2-}$** powder and **GC/CNT@p-[LCu]$^{2-}$** after 0, 1, 6 and 24 hours of CPE. The reference EXAFS spectrum of CuO is also reported for comparison purpose.

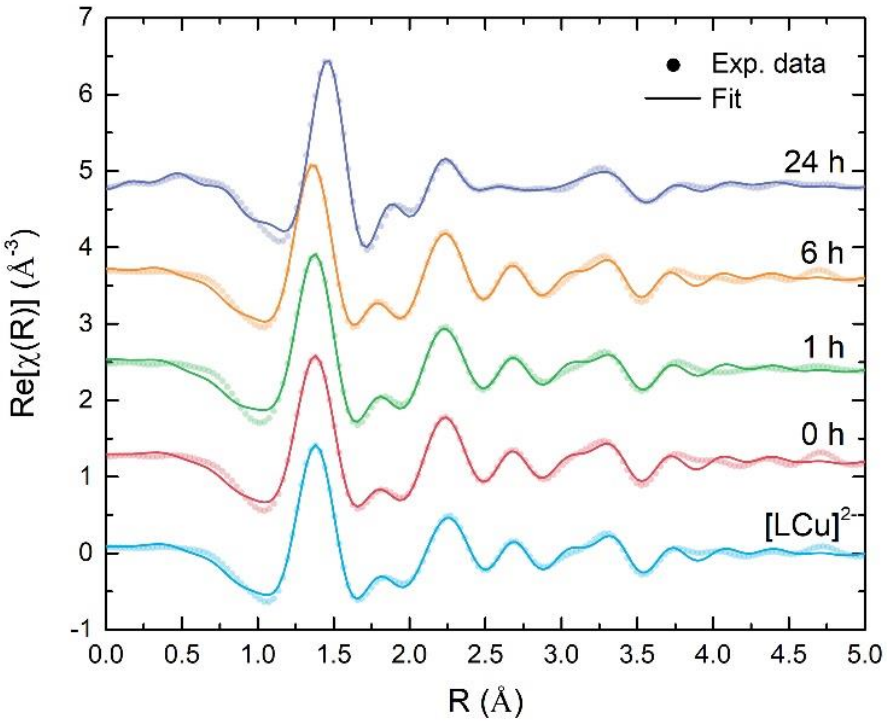

Figure S28. Real part of the experimental Fourier transforms of k2-weighted EXAFS spectra (dots) of [LCu]$^{2-}$and electropolymerized GC/CNT@p-[LCu]$^{2-}$ samples. The results of the fitting are represented as solid lines.

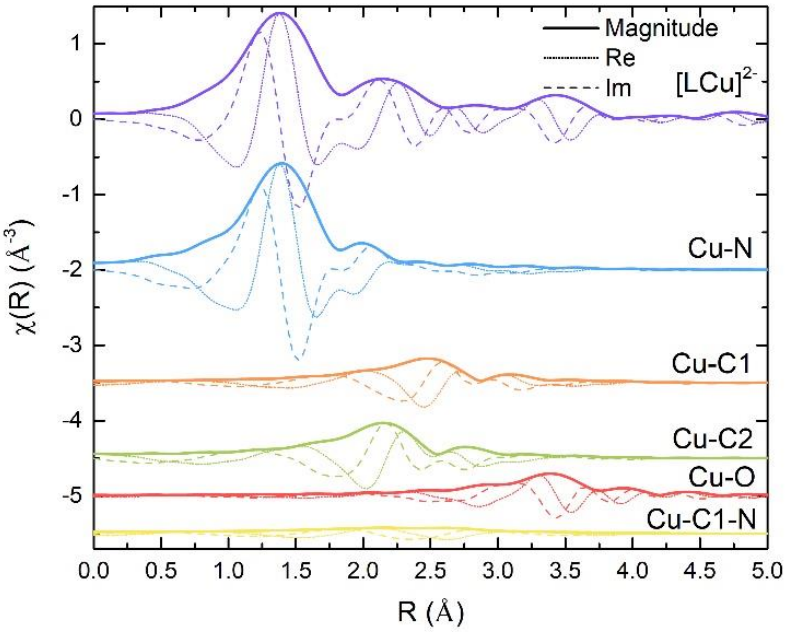

Fig. S29. Example of the Fourier transform of each scattering path that gives a significant contribution to the final model (sample $[LCu]^{2-}$). The magnitude as well as the real and imaginary parts are shown. The broad peak between 2 and 3 Å is the superposition of the contributions from the paths 2,3 and 5.

Table S2. Fit parameters obtained from the EXAFS analysis. The half path lengths R are equal to the sum of R_{eff} defined in Table S1 and the corresponding distance variation parameter ΔR. Uncertainties on the least significant figures are indicated in brackets.

Sample	Path code	R (Å)	σ^2 (Å^2)	ΔE (eV)	R-factor
$[LCu]^{2-}$	1	1.877 (4)	0.0063 (7)	3.4 (8)	0.008
	2	3.140 (28)	0.0056 (19)		
	3	2.758 (17)	0.0056 (19)		
	4	4.100 (15)	0.0003 (22)		
	5	3.123 (60)	0.014 (25)		
GC/CNT@p-$[LCu]^{2-}$ 0h	1	1.873 (4)	0.0069 (8)	3.2 (9)	0.009
	2	3.153 (24)	0.0048 (14)		
	3	2.723 (15)	0.0048 (14)		
	4	4.084 (16)	0.0000 (23)		
	5	3.09 (12)	0.029 (28)		

GC/CNT@p-[LCu]$^{2-}$ 1h	1	1.874 (4)	0.0059 (8)	4.3 (9)	0.011
	2	3.154 (25)	0.0054 (18)		
	3	2.731 (16)	0.0054 (18)		
	4	4.103 (20)	0.0008 (29)		
	5	3.0 (2)	0.046 (31)		
GC/CNT@p-[LCu]$^{2-}$ 6h	1	1.856 (4)	0.0060 (7)	2.9 (9)	0.008
	2	3.151 (23)	0.0043 (14)		
	3	2.721 (15)	0.0043 (14)		
	4	4.081 (17)	0.0000 (24)		
	5	3.05 (14)	0.030 (22)		
GC/CNT@p-[LCu]$^{2-}$ 24h	1	1.947 (4)	0.0030 (7)	4.4 (9)	0.013
	2	3.291 (56)	0.0197 (59)		
	3	2.708 (37)	0.0197 (59)		
	4	4.121 (26)	0.0037 (44)		
	5	2.900 (43)	0.0000 (62)		

References

[1] a) R. Matheu, S. Neudeck, F. Meyer, X. Sala, A. Llobet, *ChemSusChem.* **2016**, *9*, 3361-3369. b) M. Gil-Sepulcre, J. O. Lindner, D. Schindler, L. Velasco, D. Moonshiram, O. Rüdiger, S. DeBeer, V. Stepanenko, E. Solano, F. Würthner, A. Llobet, *J. Am. Chem. Soc.* **2021**, *143*, 11651–11661.

[2] F. d'Acapito, G. O. Lepore, A. Puri, A. Laloni, F. La Manna, E. Dettona, A. De Luisa, A. Martin, *J. Synchrotron Radiat.* **2019**, *26*, 551–558.

[3] B. Ravel, M. Newville, *J. Synchrotron Radiat.* **2005**, *12*, 537–541.

[4] P. Garrido-Barros, D. Moonshiram, M. Gil-Sepulcre, P. Pelosin, C. Gimbert-Suriñach, J. Benet-Buchholz, A. Llobet, *J. Am. Chem. Soc.* **2020**, *142*, 17434–17446.

[5] S. I. Zabinsky, J. J. Rehr, A. Ankudinov, R. C. Albers, M. J. Eller, *Phys. Rev. B* **1995**, *52*, 2995–3009.

[6] G. Rossi, F. D'Acapito, L. Amidani, F. Boscherini, M. Pedio, *Phys. Chem. Chem. Phys.* **2016**, *18*, 23686–23694.

[7] M. Ventosa, M. Gil-Sepulcre, J. Benet-Buchholz, C. Gimbert-Suriñach, A. Llobet, *ACS Appl. Energy Mater.* **2021**, acsaem.1c01851.